



Toward consistency between trends in bottom-up CO₂ emissions and top-down atmospheric measurements in the Los Angeles megacity

Sally Newman¹, Xiaomei Xu², Kevin R. Gurney³, Ying Kuang Hsu⁴, King Fai Li⁵, Xun Jiang⁶, Ralph Keeling⁷, Sha Feng^{8,a}, Darragh O’Keefe³, Risa Patarasuk³, Kam Weng Wong⁸, Preeti Rao⁸, Marc L. Fischer⁹, and Yuk L. Yung¹

¹Division of Geological and Planetary Sciences, California Institute of Technology, Pasadena, CA 91125, USA

²Department of Earth System Science, University of California, Irvine, CA 92697, USA

³School of Life Sciences, Arizona State University, Tempe, AZ 85287, USA

⁴Monitoring and Laboratory Division, Air Resources Board, Sacramento, CA 95811, USA

⁵Department of Applied Mathematics, University of Washington, Seattle, WA 98195, USA

⁶Department of Earth and Atmospheric Sciences, University of Houston, Houston, TX 77004, USA

⁷Scripps Institution of Oceanography, University of California, San Diego, La Jolla, CA 92037, USA

⁸Earth Atmospheric Science, Jet Propulsion Laboratory, California Institute of Technology, Pasadena, CA 91109, USA

⁹Environmental Energy Area, E. O. Lawrence Berkeley National Laboratory, Berkeley, CA 94720, USA

^anow at: Department of Meteorology, Pennsylvania State University, University Park, PA 16802, USA

Correspondence to: Sally Newman (sally@gps.caltech.edu)

Received: 9 September 2015 – Published in Atmos. Chem. Phys. Discuss.: 29 October 2015

Revised: 5 March 2016 – Accepted: 7 March 2016 – Published: 22 March 2016

Abstract. Large urban emissions of greenhouse gases result in large atmospheric enhancements relative to background that are easily measured. Using CO₂ mole fractions and $\Delta^{14}\text{C}$ and $\delta^{13}\text{C}$ values of CO₂ in the Los Angeles megacity observed in inland Pasadena (2006–2013) and coastal Palos Verdes peninsula (autumn 2009–2013), we have determined time series for CO₂ contributions from fossil fuel combustion (C_{ff}) for both sites and broken those down into contributions from petroleum and/or gasoline and natural gas burning for Pasadena. We find a 10 % reduction in Pasadena C_{ff} during the Great Recession of 2008–2010, which is consistent with the bottom-up inventory determined by the California Air Resources Board. The isotopic variations and total atmospheric CO₂ from our observations are used to infer seasonality of natural gas and petroleum combustion. The trend of CO₂ contributions to the atmosphere from natural gas combustion is out of phase with the seasonal cycle of total natural gas combustion seasonal patterns in bottom-up inventories but is consistent with the seasonality of natural gas usage by the area’s electricity generating power plants. For petroleum, the inferred seasonality of CO₂ contributions from burning petroleum is delayed by several months relative to usage indicated by statewide gasoline taxes. Using

the high-resolution Hestia-LA data product to compare C_{ff} from parts of the basin sampled by winds at different times of year, we find that variations in observed fossil fuel CO₂ reflect seasonal variations in wind direction. The seasonality of the local CO₂ excess from fossil fuel combustion along the coast, on Palos Verdes peninsula, is higher in autumn and winter than spring and summer, almost completely out of phase with that from Pasadena, also because of the annual variations of winds in the region. Variations in fossil fuel CO₂ signals are consistent with sampling the bottom-up Hestia-LA fossil CO₂ emissions product for sub-city source regions in the LA megacity domain when wind directions are considered.

1 Introduction

Carbon dioxide is the most important greenhouse gas (GHG) contributing to current global warming, contributing 64 % of the total radiative forcing, according to the IPCC AR5 report (IPCC, 2013), and comprising 82 % of GHG emissions (NRC, 2010). The global average mole fraction of CO₂ has increased approximately 40 % since pre-industrial times due

to anthropogenic emissions (IPCC, 2013). Since the proportion of the world's emissions from megacities (urban regions with more than 10 million inhabitants) is out of proportion with their small surface area (EDGAR, 2009; IEA, 2008), quantifying C_{ff} is essential if we are to work aggressively toward their reduction (Duren and Miller, 2012). As a consequence of global warming mitigation, reducing C_{ff} could reduce air pollution mortality, which is correlated with increased CO₂ levels (Jacobson, 2008).

Identifying the sources of emissions is a major first step in understanding and mitigating anthropogenic contributions. In cities, especially in megacities, these CO₂ sources often dominate over the normally predominant natural source of the biosphere, at least during certain seasons (e.g., Pataki et al., 2003; Widory and Javoy, 2003; Newman et al., 2013, 2008; Lopez et al., 2013; Turnbull et al., 2011, 2015; Vardag et al., 2015). The most common method of inventorying CO₂ emissions from human activities is through bottom-up reporting by governmental agencies, following IPCC methods (IPCC, 2013). Uncertainties in these methods range from 3 to 5 % to greater than 50 % (Andres et al., 2012). A more recent, scientifically based bottom-up approach has been pioneered through the Vulcan and Hestia projects (Gurney et al., 2009, 2012). These efforts combine multiple streams of data such as air pollution reporting, demographics, property tax data, and traffic monitoring, to arrive at what is proving to be a much more accurate and space and time detailed estimate of fossil fuel CO₂ emissions. The Vulcan Project accomplished fossil fuel CO₂ emission estimation for the whole US at spatial scales of 10 km every hour of the year 2002, with updated years expected by the end of 2015. Hestia is specifically focused on the urban domain and has accomplished estimation down to the individual building and street segment scale for four cities (Indianapolis, IN; Salt Lake City, UT; Los Angeles basin, CA; Phoenix, AZ) with work ongoing in Baltimore, MD (Gurney et al., 2012; Patarasuk et al., 2016). Both of these detailed data products are available for selected cities in the United States, facilitating top-down emissions quantification through long-term ambient air monitoring (Duren and Miller, 2012; Gurney et al., 2015). Trends in C_{ff} must be monitored precisely in order to evaluate progress towards mandated emission reductions. As an example, the California Global Warming Solutions Act of 2006 (Assembly Bill 32) requires reduction of greenhouse gas emissions to 1990 levels by 2020, a reduction of about 15 %. Indeed, now is the time to document the current level of emissions, as governments begin to implement strategies to reduce emissions (e.g., California's Cap-and-Trade Program and Low Carbon Fuel Standards) and want to be able to assess their efficacy.

Within megacities, atmospheric CO₂ concentrations are often highly elevated relative to the regional background due to locally emitted carbon dioxide. This excess can be analyzed for its isotopic composition to help attribute the local emissions to specific processes. Radiocarbon (¹⁴C) analyses give quantitative information as to the proportions of CO₂ re-

sulting from combustion of ancient sources of carbon (fossil fuels) relative to sources incorporating modern carbon, such as the biosphere (e.g., Levin et al., 2003; Levin and Roedenbeck, 2008; Turnbull et al., 2009), because of its short half-life of 5730 years. The stable isotopes of carbon can be used to separate sources with differing values, such as natural gas and petroleum combustion, with the ¹³C / ¹²C ratio of natural gas typically being lower than that of petroleum (e.g., Keeling, 1958, 1961; Clarke-Thorne and Yapp, 2003; Newman et al., 2008, 2013; Pataki et al., 2003; Widory and Javoy, 2003; Djuricin et al., 2010; Moore and Jacobson, 2015), although there can be an overlap between petroleum combustion and biological respiration. Therefore, if we know the biosphere's contribution from the fossil fuel CO₂ contribution derived from $\Delta^{14}C$ and the total CO₂ enhancement over background, we can distinguish all three sources (biosphere, petroleum combustion, and natural gas combustion) provided that there are large variations, such as in urban regions.

Here we report the use of ¹⁴C combined with $\delta^{13}C$ in flask samples to disaggregate the local emissions of CO₂ in the Los Angeles (LA) basin into biosphere, natural gas, and petroleum combustion sources. We investigate the annual patterns and trends for 2006–2013 in these components and compare them to global background and to bottom-up inventories generated by government agencies and scientific colleagues. In particular, we test the method against the changes in C_{ff} observed during and after the Great Recession of 2008–2010 in LA.

The sampling, analytical methods, and calculations are described in Sect. 2. Section 3 discusses the results with regard to spatial and temporal variations and comparison with bottom-up inventories and the detailed data product Hestia-LA. Overall conclusions are presented in Sect. 4.

2 Data and analysis

2.1 Locations

Samples were collected at two locations in the Los Angeles basin: on the campus of the California Institute of Technology (Caltech) in Pasadena, CA (34°8'12" N, 118°7'39" W, (240 ± 5) m a.s.l.), and on Palos Verdes peninsula overlooking the Pacific Ocean and Santa Catalina Island to the south (33°44.7' N, 118°20.9' W, 330 m a.s.l.) (Fig. 1). Pasadena is located in the San Gabriel valley, approximately 14 km NE of downtown Los Angeles and 40 km from the coast. Prevailing winds from the SW bring marine air from the ocean during daytime hours, as the planetary boundary layer deepens during heating of the land. During these periods of prevailing south to west winds, the Palos Verdes site is a credible background site. Since the marine air picks up emissions from the basin during its transit inland, Pasadena is a good receptor site for LA emissions. The San Gabriel Mountains just 5 km to the north act as a barrier until midday, when upslope flow

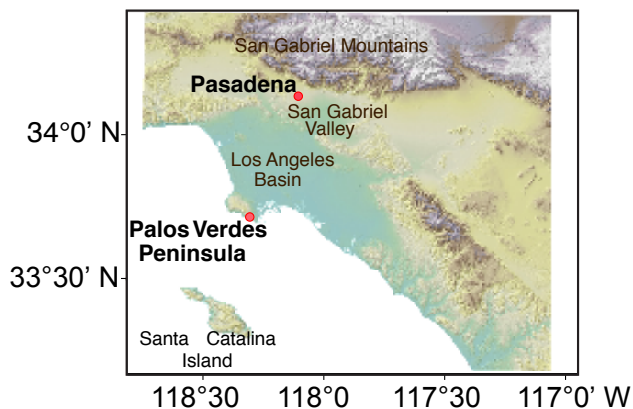


Figure 1. Map of southern California, showing sampling locations in Pasadena and Palos Verdes (red dots).

and the rising temperature inversion layer allow venting over the mountains (Lu and Turco, 1994, 1995).

2.2 Samples

Air samples were collected into evacuated 1-liter Pyrex flasks through Synflex 1300 tubing after passing through Mg(ClO₄)₂ to dry the samples. In Pasadena, samples were collected on alternate afternoons at 14:00 Pacific Standard Time (PST) using an autosampler, whereas at the Palos Verdes site samples were collected manually once a week (on weekend days) between 11:00 and 16:00 PST, and typically near 14:00 PST. The mid-afternoon sampling time was chosen because this is when the planetary boundary layer tends to be the deepest and most well-mixed during the day. The sampling path at each location was purged with ambient air before collection.

CO₂ was extracted from the air samples cryogenically, following the methods described in Newman et al. (2008), with the amount of CO₂ determined manometrically. Then the $\delta^{13}\text{C}$ was determined relative to the Vienna Pee Dee Belemnite (VPDB) standard (Coplen, 1996) by dual-inlet isotope ratio mass spectrometry (Thermo-Finnigan MAT 252; Bremen, Germany) on each individual sample. After this analysis, the CO₂ was frozen into a cold finger and combined with 3–7 other individual samples to create a composite sample characterizing mid-afternoon air over a 2-week (Pasadena) or 1-month (Palos Verdes) time period for $\Delta^{14}\text{C}$ analysis. This differs from the sampling protocol of Affek et al. (2007), who collected on average two 5 L samples per month, analyzed each sample separately, and then averaged the results to produce monthly average $\Delta^{14}\text{C}$ values for 2004–2005. We found that by combining smaller samples collected more frequently (alternate days in Pasadena) our results were less scattered than in the previous report and therefore give interpretable seasonal variations. $\Delta^{14}\text{C}$ was analyzed by accelerator mass spectrometer at the Keck-CCAMS facility at the University of California, Irvine, using the methods described

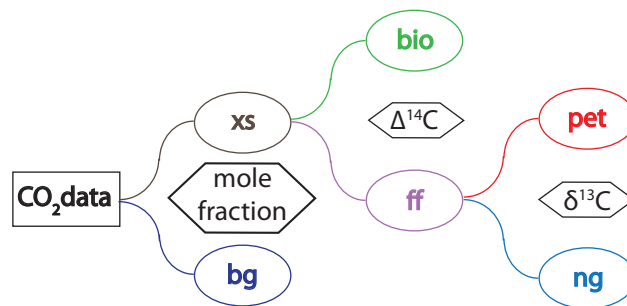


Figure 2. Schematic diagram showing the use of different data sets for attribution of the sources of CO₂ emissions. Mole fractions of background (bg) and observations are used to determine C_{xs} (excess over background/bg); $\Delta^{14}\text{C}$ values are used to distinguish C_{ff} (fossil fuel, ff) and C_{bio} (biosphere, bio); $\delta^{13}\text{C}$ compositions are used to distinguish C_{pet} (petroleum and/or gasoline, pet) from C_{ng} (natural gas, ng).

in Newman et al. (2013) and Xu et al. (2007). Analyses of air from standard tanks calibrated by NOAA (National Oceanic and Atmospheric Administration) gave errors for CO₂ mole fractions averaging of ± 1.4 ppm ($1 \text{ ppm} = 1 \mu\text{mol mol}^{-1}$) ($n = 44$) and $\delta^{13}\text{C}$ of ± 0.15 ‰ ($n = 30$), including extraction, manometry, and mass spectrometry. Although the uncertainties in the CO₂ mole fractions is much higher than by spectroscopic techniques, it contributes less than half of the total uncertainty in C_{ff}, which is dominated by the $\Delta^{14}\text{C}$ average error of 2 ‰, based on long-term reproducibility of secondary standards (Xu et al., 2007, 2010; Graven et al, 2013; Miller et al., 2013).

2.3 Calculations

A major goal of this study is the attribution of the sources of the C_{ff} observed. A schematic figure of the flow of data used to calculate the portion of the total CO₂ that is due to biosphere respiration (bio) and fossil fuel (ff) combustion, including burning of petroleum (pet) and natural gas (ng), is shown in Fig. 2. Mole fractions of CO₂ measured at the two sites and a background site in La Jolla, CA, were used to calculate the CO₂ excess (xs) over background (bg). The contributions of fossil fuel combustion and the biosphere to the excess were determined from radiocarbon measurements, and the fossil fuel component was further broken down into petroleum and natural gas using $\delta^{13}\text{C}$ of the CO₂. Details are described below.

2.3.1 Total CO₂ emissions and background CO₂ mole fraction

The CO₂ excess caused by local emissions at the two sites was calculated by subtracting an estimate of the background CO₂ mole fraction derived from La Jolla monthly values (Keeling et al., 2005; Figs. 3 and 4; Supplement). Flask sam-

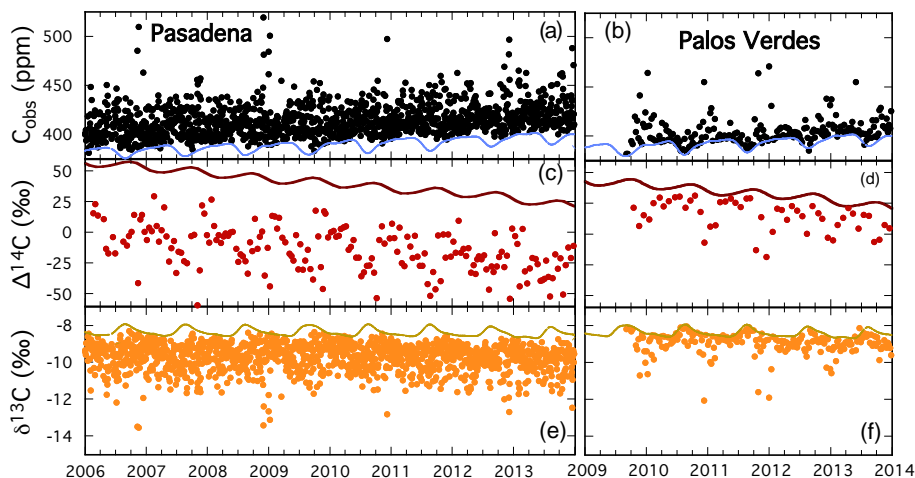


Figure 3. Time series of observed CO₂ mole fractions for ¹⁴CO₂ samples (a, b), Δ¹⁴C data (c, d), and δ¹³C (e, f) for Pasadena and Palos Verdes. The solid curves are backgrounds used in the calculations: δ¹³C and CO₂ backgrounds are from La Jolla, CA and Δ¹⁴C from Pt. Barrow, AK. Data are provided in the Supplement to this paper.

pling at La Jolla is done so as to minimize the influence of local CO₂ sources by sampling during periods that simultaneously satisfy three criteria: low variability in CO₂ concentration for periods of 3 h or more, wind speed of 2.6 m s⁻¹ or more from a narrow southwesterly to westerly sector, and high visibility. That these methods successfully minimize influences of local fossil-fuel emissions is indicated by the consistency of the annual radiocarbon concentrations at La Jolla compared to clean stations both to the north and south in the Northern Hemisphere (Graven, 2012). In this paper, therefore, the La Jolla data presented are screened background data. The La Jolla data were interpolated to determine the appropriate value for the midpoint of the range of collection dates included in each Δ¹⁴C sample, using the algorithm from Thoning et al. (1989), with two harmonic terms, three polynomial terms, and the smoothed residuals of the long-term trend (cutoff of 667 days).

2.3.2 CO₂ from fossil fuels, based on Δ¹⁴C

Mass balance calculations were used to calculate the relative contributions of background air, biosphere respiration and photosynthesis, and fossil fuel combustion (including natural gas and oil) to the CO₂ collected at the two sites. The following equations quantitatively separate the background air, biosphere, and fossil fuel combustion contributions to the locally measured atmospheric CO₂ using Δ¹⁴C (e.g., Levin et al., 2003; Miller et al., 2012; Pataki et al., 2003; Turnbull et al., 2006; Fig. 4):

$$C_{\text{obs}} = C_{\text{bg}} + C_{\text{ff}} + C_{\text{r}} + C_{\text{p}} \quad (1)$$

$$\Delta_{\text{obs}} C_{\text{obs}} = \Delta_{\text{bg}} C_{\text{bg}} + \Delta_{\text{ff}} C_{\text{ff}} + \Delta_{\text{r}} C_{\text{r}} + \Delta_{\text{p}} C_{\text{p}}, \quad (2)$$

where subscripts obs, bg, ff, r and p indicate observed, background, fossil fuels, respiration, and photosynthesis, respec-

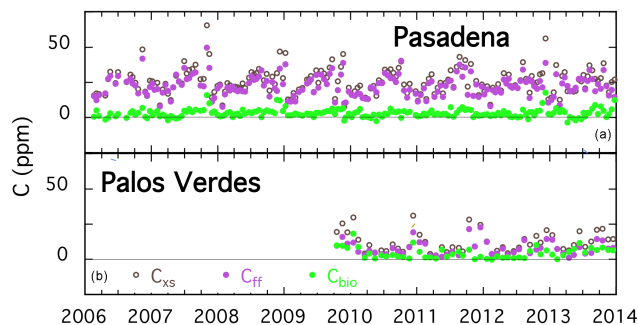


Figure 4. Time series of C_{xs} , C_{ff} , and C_{bio} calculated from Δ¹⁴C (see text for description of calculations) for Pasadena (a) and Palos Verdes (b). The errors for C_{ff} are 1 ppm. The negative C_{bio} values indicate photosynthetic uptake. The value of Δ¹⁴C for fuel for this calculation was taken to be −954 ‰, the average from the summer and winter calculations.

tively; C indicates CO₂ mole fraction in ppm, and Δ indicates Δ¹⁴C in ‰. We assume that Δ_p is equivalent to Δ_{bg} since natural fractionation during uptake is corrected in the Δ¹⁴C measurement and therefore substitute Δ_{bg} for Δ_p in Eq. (2). Then, after solving Eq. (1) for C_{p} and substituting this for C_{p} in Eq. (2), we solve Eq. (2) for C_{ff} , resulting in the following expression for C_{ff} :

$$C_{\text{ff}} = \frac{C_{\text{obs}} (\Delta_{\text{obs}} - \Delta_{\text{bg}})}{\Delta_{\text{ff}} - \Delta_{\text{bg}}} \frac{C_{\text{r}} (\Delta_{\text{r}} - \Delta_{\text{bg}})}{\Delta_{\text{ff}} - \Delta_{\text{bg}}}. \quad (3)$$

The value of Δ_{ff} is −1000 ‰, since fossil fuels contain no ¹⁴C because they have been removed from the source of this short-lived radionuclide for millions of years.

We use the record from Pt. Barrow, AK (Xiaomei Xu, unpublished data) for the concurrent background Δ¹⁴C values (Δ_{bg}), because this is the most complete record available for

the entire time period of this study. The background $\Delta^{14}\text{C}$ record at Pt. Barrow, AK is obtained through the UCI/NOAA ESRL (Earth System Research Laboratory) flask network program that collects whole air samples using 6 L, one-valve stainless steel canisters (Silco Can, Restek Co.) that have been pre-evacuated at UCI. The canisters are pressurized to ~ 2 atm using an oil-free pump. Two biweekly samples were collected before 2008, and one weekly afterwards. For the period from 17 June 2005 to 17 March 2006, some duplicate samples were collected using 32 L, one-valve stainless steel canisters. Subsamples were then taken from these samples for ^{14}C analysis. CO₂ is extracted cryogenically at UCI then converted to graphite by the sealed tube zinc reduction method (Xu et al., 2007). Each sample is ~ 2.7 mg C in size. Analysis of $\Delta^{14}\text{C}$ is performed at the W M Keck AMS facility at UCI with a total measurement uncertainty of ± 1.3 – 2.4 ‰. Mass dependent fractionation is corrected for using “on-line” $\delta^{13}\text{C}$ measurements during AMS analysis, which accounts for fractionation that occurred during graphitization and inside the AMS. Comparison was made of 22 common sample dates spanning 5 years, of measured $\Delta^{14}\text{C}$ from Barrow between the UCI and the Scripps Institution of Oceanography’s CO₂ Program. It shows that differences in measured $\Delta^{14}\text{C}$ are consistent with the reported uncertainties and there is no significant bias between the programs (Graven et al., 2013). Another inter-comparison is that of AMS-based atmospheric $^{14}\text{CO}_2$ measurements organized by the NOAA Earth System Research Laboratory, Boulder, Colorado. The UCI lab is one of the three groups having inter-laboratory comparability within 1 ‰ for ambient level $^{14}\text{CO}_2$ (Miller et al. 2013). Comparison of the Pt. Barrow data with those from La Jolla (Graven et al., 2012; Fig. 5) shows good agreement for 2004–2007, when the two data sets overlap. Comparing the calculated values for C_{ff} from these two backgrounds and propagating through the time series calculations (Sect. 3.4) results in a difference of approximately 1 % of the signal we are measuring. We calculate C_{bio} (the sum of C_{r} and C_{p}) from Eq. (1), using the calculated values of C_{ff} and the independent estimates of C_{bg} from the La Jolla data, so that we understand the contribution of the biosphere to total local emissions.

The nuclear power plant contribution, the only other source of ^{14}C , is small on the west coast of the US (Graven and Gruber, 2011) and therefore is ignored.

Following Turnbull et al. (2006) and Miller et al. (2012), the respiration terms in the equations above are assumed to reflect contributions due to heterotrophic respiration. Thus, the second term in Eq. (3) is small in magnitude and is due to heterotrophic respiration, through which microbes respire CO₂ that was from carbon previously incorporated through photosynthesis. This term takes into account the isotopic disequilibrium due to the significant time delay between photosynthetic incorporation and respiration, assumed to be 10 years on average (Miller et al., 2012). The magnitude of this correction for our urban Pasadena site is different rela-

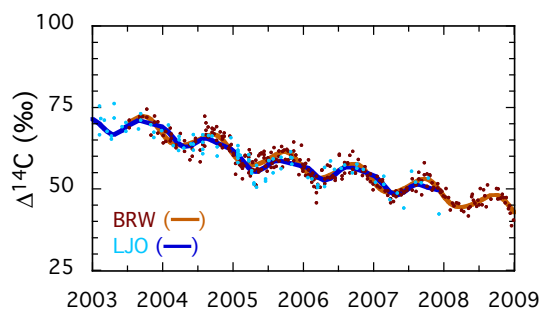


Figure 5. Comparison of possible background records for this study, Pt. Barrow, AK, (BRW; Xiaomei Xu, unpublished data) and La Jolla, CA (LJO; Graven et al., 2012). The smoothed brown curve for BRW is the $\Delta^{14}\text{C}$ background used for this study and was calculated using the algorithm of Thoning et al. (1989), from the function plus the smoothed residuals of the long-term trend, using two harmonic and three polynomial terms in the function and 667 days as the long-term cutoff for the low-pass filter.

tive to sites with smaller anthropogenic CO₂ signals, since the CO₂ photosynthesized into the plant a decade ago was not close to the background air composition of that time but was the local, “polluted” air. The Δ_{r} in Eq. (3) for each sample was calculated by extrapolating the Pasadena trend back 10 years. Because of the mild climate in southern California, we used a constant value of $C_{\text{r}} = 5$ ppm, the same value used for summer by Turnbull et al. (2006). This should be taken as an upper limit for this urban region. The range of the correction for the second term in Eq. (3), including the sign, was -0.06 to -0.11 ppm, generally smaller relative to regions where the biosphere contribution C_{r} is large (Miller et al., 2012; Turnbull et al., 2006). For the data from the Palos Verdes site, we calculated the heterotrophic correction term using values of Δ_{r} calculated by extrapolating the Pt. Barrow background trend back 10 years and used a constant value of $C_{\text{r}} = 5$ ppm, because of the mild climate. The correction term for the Palos Verdes data ranged from 0.20 to 0.24 ppm. The small correction for heterotrophic respiration does not affect any of our conclusions.

In California, there is an added complication when attributing CO₂ emissions to fossil fuels using $\Delta^{14}\text{C}$. Since 2004, 10 % ethanol has been added to gasoline. The ethanol contains modern, not fossil, carbon. For gasoline with 10 % ethanol, 6.7 % of the CO₂ emitted during combustion is from the modern ethanol (EIA, 2015). A correction for this is made, as discussed in Sect. 2.3.3 below.

2.3.3 $\delta^{13}\text{C}$ of CO₂

Plots involving the mole fractions and $\delta^{13}\text{C}$ can be used to determine $\delta^{13}\text{C}$ of the local contribution to the observed CO₂ (Fig. 3). Here we use the Miller–Tans approach (Miller–Tans approach; MT; Miller and Tans, 2003) for this purpose, since it allows for variations in background composition and we

observe a widening difference between the data for $\delta^{13}\text{C}$ in Pasadena and the La Jolla background record in recent years (Fig. 3e). The following mass balance equations are used in this analysis:

$$C_{\text{obs}} = C_{\text{bg}} + C_{\text{src}} \quad (4)$$

$$\delta_{\text{obs}} \times C_{\text{obs}} = \delta_{\text{bg}} \times C_{\text{bg}} + \delta_{\text{src}} \times C_{\text{src}} \quad (5)$$

to give

$$\delta_{\text{obs}} \times C_{\text{obs}} - \delta_{\text{bg}} \times C_{\text{bg}} = \delta_{\text{src}}(C_{\text{obs}} - C_{\text{bg}}), \quad (6)$$

(Miller and Tans, 2003) where the subscript src represents the local source of CO₂ emissions, δ represents $\delta^{13}\text{C}$, and the appropriate background values are included for each sample. Using this formulation (Eq. 6), the slope of the correlation (MT slope) gives the $\delta^{13}\text{C}$ of this local source. For this analysis, we calculated the MT slopes for each month and then determined the seasonal averages, averaging December–January–February as winter, March–April–May as spring, June–July–August as summer, and September–October–November as autumn. Seven individual samples, over the 8-year sampling period in Pasadena, were excluded since they fell more than three times the standard error from their linear regression best-fit lines. The monthly MT plots for 2011 are shown in Fig. A1 in the Appendix, as examples. The very high correlation coefficients ($R = 0.952$ – 0.999) suggest that δ_{src} remains constant on timescales of a month. We assume that this is also the case for the isotopic compositions of petroleum and natural gas combustion, that we describe below.

We use the results from the ¹⁴CO₂ calculations for the fraction of C_{xs} from the biosphere ($F_{\text{bio}} = 1 - F_{\text{ff}}$) together with the MT slopes to attribute the CO₂ derived from petroleum and natural gas combustion (C_{pet} and C_{ng}) by mass balance, first by calculating the $\delta^{13}\text{C}$ of the fossil fuel component, using

$$\delta_{\text{ff}} = \frac{\delta_{\text{xs}} - \delta_{\text{bio}} \times (1 - F_{\text{ff}})}{F_{\text{ff}}}, \quad (7)$$

where F_{ff} is the fraction of C_{xs} due to emissions from fossil fuel combustion, as calculated from the ¹⁴CO₂ data. The values for δ_{xs} are the seasonal $\delta^{13}\text{C}$ values from the MT analyses and δ_{bio} is taken to be -26.6‰ , the average $\delta^{13}\text{C}$ of the ambient air plus the discrimination of -16.8‰ for the biosphere (Bakwin et al., 1998). This value represents data from temperate northern latitudes (28 – 55°N), dominated by C3 plants with some C4 grasses present (Bakwin et al., 1998). Indeed, grasses in southern California are mostly C3 ryes, fescue, and bluegrass, with some C4 grasses such as St. Augustine (www.cropsreview.com/c3-plants.html, last access: 25 January 2016). The proportions of CO₂ emitted by petroleum and natural gas combustion are calculated us-

ing the $\delta^{13}\text{C}$ values:

$$\delta_{\text{ff}} = F_{\text{pet ff}} \times \delta_{\text{pet}} + (1 - F_{\text{pet ff}}) \times \delta_{\text{ng}} \quad (8)$$

$$F_{\text{pet ff}} = \frac{\delta_{\text{ff}} - \delta_{\text{ng}}}{\delta_{\text{pet}} - \delta_{\text{ng}}}, \quad (9)$$

with an analogous equation for $F_{\text{ng ff}}$, where $F_{\text{pet ff}}$ and $F_{\text{ng ff}}$ are the fractions of petroleum and natural gas combustion contributions in C_{ff} , respectively. The values of δ_{ng} and δ_{pet} used were $-40.2 \pm 0.5\text{‰}$ for natural gas (Newman et al., 2008; covering measurements in 1972–1973 and 1999) and $-25.5 \pm 0.5\text{‰}$ for petroleum combustion (average of measurements in Newman et al. (2008); measurements in 2005), and -26.0 , -25.1 , and -25.5‰ measured in 2007, 2012, and 2014, respectively). The C_{ff} , C_{pet} , and C_{bio} components were corrected for the presence of 10 % ethanol in California gasoline by multiplying C_{pet} by 0.067 (the fraction of CO₂ emitted by burning the ethanol portion of the ethanol-gasoline mixture; EIA, 2015) to give the amount, in ppm, of CO₂ that was included in C_{bio} but should have been attributed to C_{pet} . The same amount was deducted from C_{bio} . The magnitude of this correction is 0.5–1.2 ppm, averaging 0.84 ppm, which represents approximately a quarter of the C_{bio} , but the latter is very small, averaging 3–4 ppm and the correction does not affect our results with respect to C_{pet} and C_{ng} .

2.3.4 Time series analysis

We used the algorithm of Jiang et al. (2008) to study details of the average annual patterns of the total CO₂ and C_{ff} in Pasadena, in order to compare with patterns at sites with less contribution from regional fossil fuel combustion, such as Palos Verdes and La Jolla background. This method uses the first three Legendre polynomials and harmonic terms to decompose the signal (Prinn et al., 2000). The harmonic terms define the seasonal and semi-annual cycles, which we compared to results of the same analysis for flask data from La Jolla, CA (Keeling et al., 2005).

To determine trends in the C_{ff} time series, derived from the radiocarbon data, we used the empirical mode decomposition (EMD) method (Huang et al., 1998; Kobayashi-Kirschvink et al., 2012). Using this method, nonlinear and nonstationary time series can be broken down into intrinsic mode functions (IMFs) with increasing period lengths and, finally, to a long-term trend with at most only one minimum or maximum with slope of zero. The algorithm involves using cubic splines to calculate maximum and minimum envelopes for the data series. The average of these envelopes for each time is subtracted from the original or the previous iteration. This process is repeated until the average is a horizontal line, giving the first IMF. This IMF is subtracted from the raw time series (or previous starting point) and then repeated until the resulting IMF has only one maximum or minimum in the series, the long-term trend. High-frequency modes are removed first, with the earliest representing noise. The later modes are

interpreted in terms of known processes, such as annual cycles (e.g., IMFs 3 and 4). Following Wu and Huang (2009), we added random noise equivalent to the error in the measurements to create 300 time series, for which the ensemble EMD (EEMD) analyses were averaged. The EEMD technique is data adaptive, not assuming any shape for the IMFs.

3 Results and discussion

The purpose of this project was to determine the sources of C_{ff} in the Los Angeles basin and compare them with bottom-up inventories and data products from government agencies and the scientific community. Below, we compare results of source allocation from the two sites and then examine the temporal variability at the Pasadena site, with its 8-year record. Then we compare the results with government inventories and with the high-resolution Hestia-LA emissions product.

3.1 Spatial variations – comparison of source attribution at the Pasadena and Palos Verdes sites

The $\Delta^{14}C$ time series for the two sites are shown in Fig. 3c and d, 8 years for Pasadena and 4 years for Palos Verdes. The two data sets are very different, with Palos Verdes radiocarbon results being significantly higher than those in Pasadena except during the winter. However, the summer months in Pasadena are characterized by $\Delta^{14}C$ values far from background, i.e., depleted in ^{14}C due to dilution by CO₂ produced by burning of fossil fuels containing none of the radioactive isotope. There are occasional negative spikes in $\Delta^{14}C$ during the winter. Total CO₂ excess (C_{xs} ; Fig. 4), determined as CO₂ concentration minus background, is similarly disparate with respect to timing. The total enhancement at both Pasadena and Palos Verdes, C_{xs} , spikes during winter (up to 65 and 34 ppm, respectively), but the Pasadena excess also peaks during the summer (up to 43 ppm), whereas Palos Verdes values for C_{xs} are at a minimum during the warm months (3–20 ppm). When the ^{14}C and C_{xs} information are combined to calculate CO₂ emissions due to fossil fuels (C_{ff} ; Eq. (3); Fig. 4), we see summer maxima for C_{ff} in Pasadena, but not in Palos Verdes. The spikes in C_{xs} and C_{ff} during autumn and winter seasons are not the general trend in Pasadena, as evidenced by the quarterly averages (Fig. 6b). The amount of C_{ff} in the Pasadena seasonal averages (Figs. 4a, 6b) ranges from (18.9 ± 1.2) ppm (winter) to (26.8 ± 0.4) ppm (summer). In Palos Verdes, C_{ff} averages (5 ± 3) ppm during the warmer months and (12 ± 5) ppm during the winter months (Fig. 4b). However, CO₂ emissions from the biosphere (C_{bio}) tend to be higher during the cooler months at both sites (Fig. 4). Refer to Sect. 3.2 for more discussion of the biosphere's contribution to C_{xs} in Pasadena.

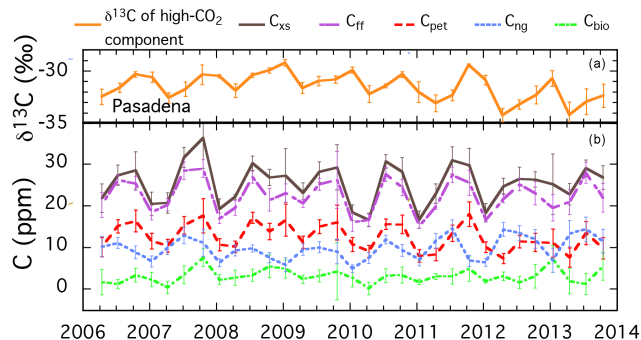


Figure 6. Attribution of CO₂ excess in Pasadena among combustion of natural gas and petroleum and the biosphere. **(a)** Miller-Tans slopes for seasonal averages of monthly plots. Error bars are standard errors of the regression intercepts. **(b)** Attribution of C_{xs} among all three sources (natural gas, petroleum, and the biosphere), combining the information from $\Delta^{14}C$ and $\delta^{13}C$, using Miller-Tans slopes to determine the relative proportions of petroleum and natural gas combustion. Error bars are propagated from the errors in the $\delta^{13}C$ intercepts and the $\Delta^{14}C$ measurements.

The explanation for the differences in the seasonal cycles of C_{xs} and C_{ff} at the two sites is probably the different wind patterns for the different times of year. Figure 7 shows back trajectories ending at 14:00 PST in Pasadena (Fig. A2 for both sites), calculated using NOAA's HYSPLIT model (Draxler and Rolph, 2014; Rolph, 2014), for January and July 2011. These back trajectories are representative of these months in all years of this study. Wind directions during July are from the west-southwest, whereas they are mostly from the northeast but much more varied during the winter. Thus, in Pasadena, elevated C_{xs} and C_{ff} values during the summer result from air masses traveling across the Los Angeles basin, picking up emissions and transporting them inland. During the winter, the airflow is more mixed, resulting in lower average C_{ff} signals in Pasadena, since a significant proportion of the winds bring less polluted air from the much less populated mountains and deserts located to the north (Santa Ana winds) (Fig. 7). The summer westerly winds bring ocean air to the Palos Verdes site, characterized by CO₂ mole fractions and $\Delta^{14}C$ very similar to background marine air. During the cooler months, the Santa Ana winds from the northeast occasionally blow over the LA basin, bringing its emissions to the coastal site (Fig. 7; Raphael, 2003; Conil and Hall, 2006). This pattern results in more scatter in the magnitude of CO₂ excess observed during the winter at the Palos Verdes site, than during the summer. Figure 8 shows the average annual pattern for C_{ff} at the two sites, demonstrating the effect of the varying wind direction patterns.

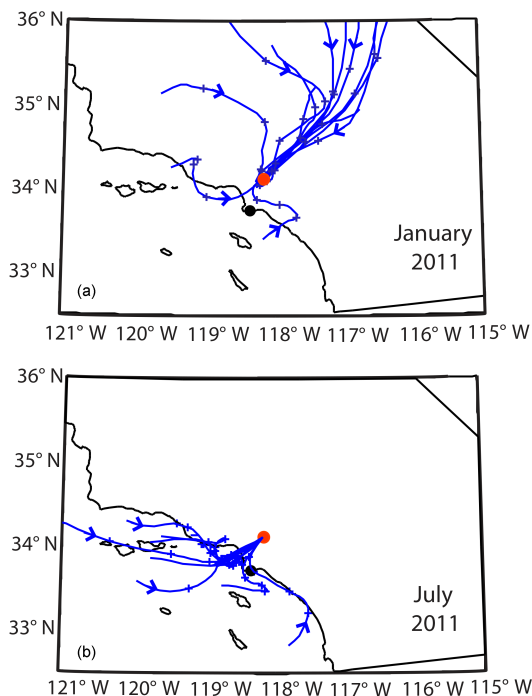


Figure 7. Back trajectories (24 h) for winds arriving at the Pasadena site (red dot) at 14:00 PST for January (a) and July (b) 2011, calculated by HYSPLIT (Draxler and Rolph, 2015; Rolph, 2015) for all sampling days in January and selected sampling days in July, for clarity. Results for all sampling days are shown in Fig. A2. Arrows indicate the direction of air flow. Plus signs indicate 6, 12, and 18 h from the Pasadena site. The black dot is the location of the Palos Verdes site. The back trajectories for the Palos Verdes site show a similar pattern (Appendix Fig. A2). The back trajectories explain the difference between the annual cycles at the two sites, shown in Fig. 8.

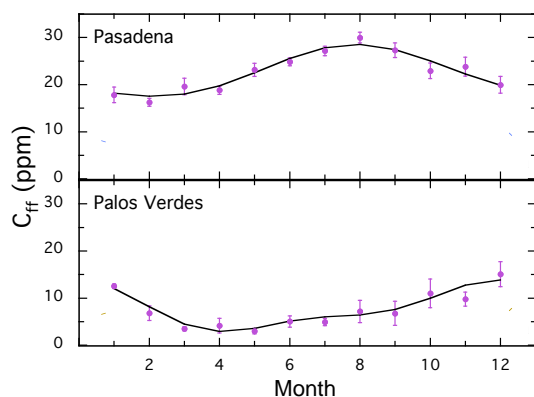


Figure 8. The annual patterns for C_{ff} in Pasadena and Palos Verdes calculated as the best fit of two harmonics plus the average of the annual cycles (black curves). These patterns are consistent with seasonal differences in the back trajectories shown in Fig. 7.

3.2 Attribution of CO₂ excess from different anthropogenic sources for Pasadena

Since we have information regarding the relative contributions of fossil fuel combustion and biosphere respiration from the radiocarbon data, we can use the differences in the $\delta^{13}\text{C}$ of the CO₂ to look at the contributions of petroleum/gasoline versus natural gas combustion. We use the MT approach to distinguish between different fossil fuel sources of CO₂ (Miller and Tans, 2003). As described in Sect. 2.3.3, the MT slope of the correlation gives the $\delta^{13}\text{C}$ of the local source of CO₂ emissions. In many cases it is difficult to distinguish the anthropogenic sources because the biosphere's signal can overlap that of petroleum. However, in a megacity such as the Los Angeles basin, the contribution of the biosphere to the total CO₂ enhancement can be minimal ($\leq 20\%$ in Pasadena; Newman et al., 2008, 2013) during the afternoon, when the boundary layer is deepest and most thoroughly mixed. In this study, we use the information from $\Delta^{14}\text{C}$ presented above to further constrain the biosphere's input. Since the other major anthropogenic sources (cement production and combustion of coal) are not present in the Los Angeles basin, $\delta^{13}\text{C}$ from MT plots can be used to differentiate the proportions of natural gas and oil burned in the region, as discussed below.

Seasonal MT slopes for the mid-afternoon Pasadena samples from 2006 through 2013 are shown in Fig. 6a. We do not present similar analysis for the Palos Verdes data because it is a shorter data set, with only 3–5 measurements per month (12 per season), and the range in CO₂ mole fractions during the warmer months is less than 20 ppm for all spring and summer seasons. Thus there are insufficient meaningful data to produce a significant trend. Vardag et al. (2015) came to this same conclusion for a rural site in Germany, based on a modeling study.

The $\delta^{13}\text{C}$ values from MT regressions for the cooler portions of the year in Pasadena are almost always higher than those for the warmer portions. The values for the cooler seasons average $(-30.6 \pm 0.5)\text{‰}$, 1.8‰ higher than the average for the warmer months, $(-32.4 \pm 0.6)\text{‰}$. Assuming that there is no contribution from respiration and that the $\delta^{13}\text{C}$ of the high-CO₂ end members are -40.2‰ for natural gas and -25.5‰ for petroleum combustion, as discussed above, then the proportion of natural gas burned in C_{xs} is 32% during the cooler months and 45% during the warmer months. The larger fraction of natural gas burned during the warm part of the year is consistent with the observed burning of more natural gas for electricity generation during summer months, as would be required to power air conditioning needs. Mild winters in this climate require less natural gas combustion for heating buildings, thus minimizing a large winter peak frequently seen in colder regions, such as Salt Lake City, UT (Pataki et al., 2003; Bush et al., 2007) and Chicago, IL (Moore and Jacobson, 2015). This attribution of the different contributions to C_{ff} still does require knowledge of the $\delta^{13}\text{C}$

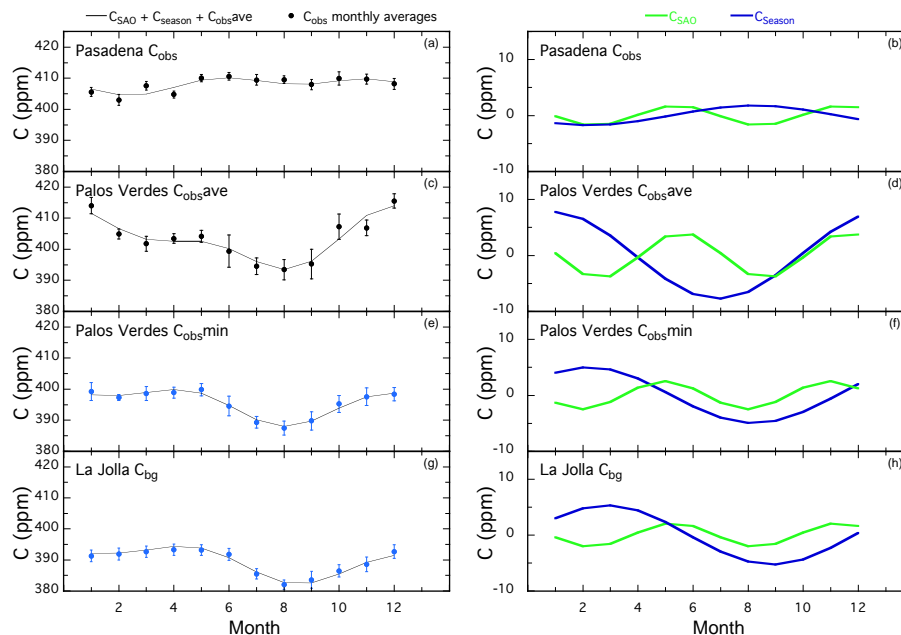


Figure 9. Comparison of seasonal and semi-annual oscillation cycles of CO₂ mole fractions for flask samples from Pasadena (2006–2013) with those at the La Jolla (2006–2013) and Palos Verdes (2009–2013) sites. Panels (a, c, e, g) show the average annual patterns for the monthly averages together with the sum of the harmonics for seasonal (blue) and semi-annual (green) cycles (Jiang et al., 2008). Panels (b, d, f, h) show the amplitudes and phases of the pure harmonic components. Two sets of results are shown for Palos Verdes, for the monthly averages (c, d) and for the monthly averages of weekly minima (e, f). The monthly averages show the effect of transport on the signal, with a large peak during the winter, while the minima (in blue) show that data from this site are very similar to La Jolla (in blue) and should be a good estimation of the background air for the LA basin. Error bars on the monthly averages of the data are 1σ standard errors.

value of the biosphere. As mentioned above, we use a discrimination of 16.8‰, the average determined by Bakwin et al. (1998) for northern mid-latitudes and includes a mix of C3 and C4 metabolism plants, dominated by C3. More C4 plants will raise the C_{ng} curve and lower the C_{pet} curve, since the discrimination by C4 plants is much lower (Farquhar et al., 1989).

As mentioned above, we can use the information provided by the ¹⁴CO₂ data to put better constraints on contributions from the biosphere. The calculations based on $\Delta^{14}C$ data in Fig. 6b show that the maximum biosphere contribution was during winter 2012–2013, 7 ppm (28% of the total C_{ff}), and the minimum was 0.1 ppm during spring of 2010. The average is (4.1 ± 0.5) ppm (16% of C_{ff}) during cooler months and (2.2 ± 0.3) ppm (8% of C_{ff}) during warmer months. The seasonality could be due to variations in emissions from the biosphere. However, it is probably due to a more complex combination of emissions and uptake.

The observation that there are seasonal patterns to the CO₂ emissions from combustion of petroleum and natural gas has implications for the effective composition of $\Delta^{14}C$ from fuel combustion. The value for fossil fuels is taken to be -1000 ‰, since they contain no ¹⁴C. However, because we have 10% modern ethanol in our gasoline, and there is seasonal variation in the ratio of gasoline to natural gas usage,

there is actually a seasonal variation in radiocarbon from the bulk fuel combustion component. And at no time is the $\Delta^{14}C$ value actually that of pure fossil fuel (-1000 ‰). The average value is -954 ‰, and spring–summer periods average 33‰ higher than autumn–winter (-939 to -972 ‰, respectively). These seasonal and overall values for $\Delta^{14}C$ of the fuel component were determined as the best-fit values from the individual C_{ff} data to the seasonal mass balance calculations of C_{pet} and C_{ng} .

3.3 Average seasonal and semi-annual patterns

The emissions of CO₂ by anthropogenic processes significantly modifies the annual cycle of CO₂ observed in the Los Angeles region relative to the oceanic air that enters the basin, as exemplified by the background air sampled in La Jolla, CA (Keeling et al., 2005; see discussion in Sect. 2.3.1). There is very little seasonal variability in Pasadena (Fig. 9a). Whereas the average background annual cycle is characterized by a peak in April and drawdown in August–September, with an amplitude of 11 ppm (Fig. 9g), the Pasadena cycle is noisy and relatively flat, with lower CO₂ mole fractions in January–April and high values the rest of the year and only an amplitude of 5 ppm (Fig. 9a). Each pattern can be modeled well using the Legendre polynomial and/or harmonic analysis of Jiang et al. (2008; Fig. 9b, h). The sum of the seasonal

and semi-annual harmonic terms reproduces the data very well, with r^2 values of 0.70 and 0.91 for Pasadena and background, respectively. The average annual cycles are 6 months out of phase, whereas the semi-annual oscillation cycles look very similar at the two sites. The seasonal cycle in Pasadena is consistent with influx of combustion CO₂ during the hot summer months due to increased burning of natural gas at power plants located dominantly in the southwestern portion of the LA basin (CEC, 2015). In contrast, the background data reflect global patterns with a drawdown in CO₂ during the summer growing season in the Northern Hemisphere. Jiang et al. (2012) concluded that the semi-annual oscillation at NOAA's GLOBAL-VIEW sites is due to the combination of gross primary production and respiration of the biosphere. During the winter season, photosynthesis is largely reduced. The peak for gross primary production is relatively flat in winter. However, CO₂ is still emitted to the atmosphere by respiration from the biosphere in winter, which has a relatively sharp peak compared with the photosynthesis term. Thus the combination of gross primary production and respiration leads to the double peaks in each year in the net ecosystem production, which contributes to the semi-annual oscillation in CO₂ (Jiang et al., 2012). The semi-annual oscillation in the background signal is consistent with this interpretation. We see virtually the same pattern in Pasadena, although the amplitude is smaller, consistent with the small biospheric contribution indicated by the $\Delta^{14}\text{C}$ results.

Based on the work of Jiang et al. (2012) we expect the annual cycle in Pasadena to be larger in amplitude than in La Jolla since it is further north, but the amplitude is actually much smaller. If the regional emissions of CO₂ in Pasadena are relative to a La Jolla background, then there is a huge enhancement during the summer! Indeed, the seasonal cycle for C_{ff} (Fig. 8) is 11 ppm, with the peak in August–September, and there is very little semi-annual oscillation.

The annual pattern for CO₂ in Palos Verdes is also heavily influenced by the transport of combustion emissions from the Los Angeles basin (Figs. 7, 8, 9c, d). The average monthly pattern is more similar to the background's (Fig. 9g, h) than to Pasadena's (Fig. 9a, b). However, there is a strong peak in the winter that is consistent with the increased number of days during this time of year with winds from the north to east traveling over the basin. Doing the same analysis for the monthly minimum values (Fig. 9e, f) gives a pattern that is much more similar to the background's, confirmed by the comparison of the raw data with the background smoothed time series in Fig. 3. This supports use of minimum values from Palos Verdes as reasonable background for the Los Angeles basin. The C_{ff} annual pattern is inverse to that in Pasadena, as expected by the seasonal wind patterns (Figs. 7, 8).

The conclusion of this analysis of the annual cycles is that the Pasadena CO₂ pattern is significantly different from the natural cycles observed in La Jolla background and show very little seasonal variation compared with this background.

The semi-annual pattern, although smaller in amplitude than expected, is in phase with that observed in the background, which we suggest might reflect a reduced biosphere signature in Pasadena due to artificial irrigation, which may reduce seasonality expected due to wet and dry parts of the year. Both the Pasadena and Palos Verdes average CO₂ patterns reflect the seasonal changes in wind patterns, whereas the monthly minimum Palos Verdes pattern is that expected for the background air entering the LA basin. It will be interesting to see whether water restrictions put into effect during summer of 2015 because of an on-going, severe drought (ca.gov/drought, 2015) affect the patterns observed in the future.

3.4 Temporal trends in CO₂ excess observed in Pasadena

3.4.1 Long-term time series analysis

In order to discern the long-term trends in fossil-fuel CO₂ excess, we must first remove noise and the periodic signals discussed above from the record. We used empirical mode decomposition (EEMD; Huang et al., 1998; Kobayashi-Kirschvink et al., 2012), as described in the calculation section above, on the 8-year time series of C_{ff} (Fig. 4a) to identify intrinsic mode functions (IMFs; summary in Fig. 10a–d; full results in Fig. A3). The noise is represented by the first and second modes (IMF 1 and IMF 2). Combination of the third and fourth modes of the C_{ff} time series (IMF 3 and IMF 4) correlates significantly with the 30-day average record for temperature measured at the top of the nine-storey library next to the sampling site ($r^2 = 0.6$). Note that there are severe mode mixing problems in IMF3 (e.g. during 2011–2013) between the dominant annual cycle and subseasonal variations, which also affects the nonlinear decompositions in the higher modes. To minimize the effects of mode mixing on the extractions of inter-annual trends, we perform the EEMD again after removing the average annual cycle (minus the mean of the raw data), defined as monthly averages over the entire time period (2006–2013; resulting time series shown in Fig. 10e). The revised inter-annual trend is shown in Fig. 10f. The sum of the trend + IMF 6 is a curve with increasing C_{ff} values leading up to mid-2007, when they began to fall, until leveling off in 2010 and perhaps starting to rise towards the end of the time series. There are end effects in this method, such that we do not have confidence in the first and last years of the analysis. The uncertainties in this calculation are shown by the shaded regions in Fig. 10f. These were determined as the 1σ standard deviations of adding random noise equivalent to 13.7 % to the data 300 times and then running the EMD analysis. The 13.7 % noise added is the uncertainty of the C_{ff} values calculated from $\Delta^{14}\text{C}$, ± 1 ppm, relative to the standard deviation of the data, 7.3 ppm. The maximum and minimum values are distinct at approximately the 2σ standard deviation level, as shown in Fig. 10f and indi-

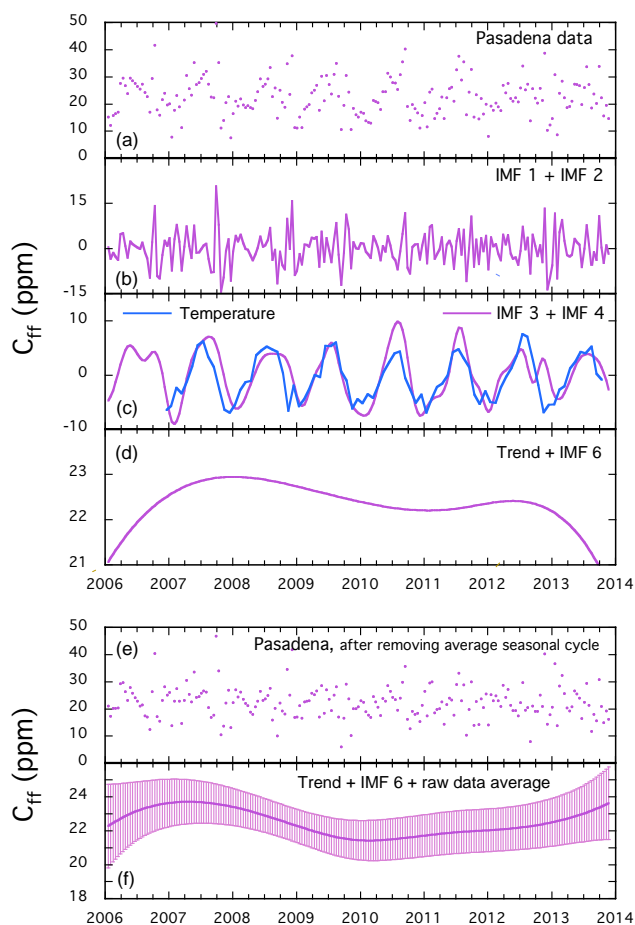


Figure 10. Results of ensemble empirical mode decomposition (EEMD) (Huang et al., 1998; Wu and Huang, 2009) of the C_{ff} time series calculated using Eq. (3) and the average, constant $\Delta^{14}C$ of -954‰ for fossil fuel. The top set of panels show the raw data (a), noise (b), annual and semi-annual mode (c), and the trend + IMF 6 (d). The pattern of the trend + IMF 6 shown in (d) is within 1σ uncertainty of no variation over this time period. The bottom two panels include the raw data after subtracting the average annual cycle (centered at zero) (e) and the trend + IMF 6 for the modified data set (f). 30-day average temperatures (minus the overall average and scaled to match the magnitude of the C_{ff} IMF; blue curve) are superimposed on the plot of IMF 3 + IMF 4 (c). Shaded regions in (f) indicate 1σ standard deviation of 300 Monte Carlo realizations with 13.7% noise added, the ratio of the uncertainty in C_{ff} to the standard deviation of the data.

cate a significant decrease of 9.5% between the maximum in May 2007 and the average for January–June 2010. Using different backgrounds for $\Delta^{14}C$, such as extrapolating the data from La Jolla (Fig. 5) does not significantly affect this analysis, resulting in differences of (0.01 ± 0.09) ppm C_{ff} out of a range on the order of 2 ppm. And our result showing that there are different values of $\Delta^{14}C$ for bulk fuel for autumn–winter than for spring–summer also does not change these conclusions, since the RMSE of the IMF6 + trend (Fig. 10f)

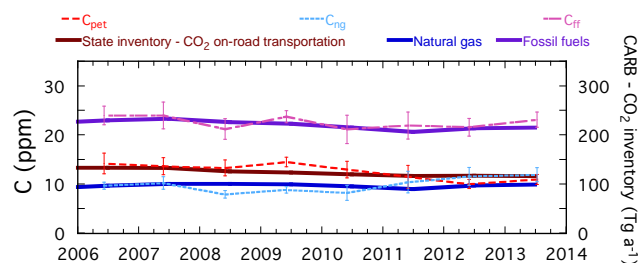


Figure 11. Comparison of annual average CO₂ emissions from bottom-up California Air Resources Board (CARB) inventories (thick lines; right axis labels) for fossil fuel-derived emissions with top-down annual averages from the Pasadena data, using the Miller and Tans (2003) approach to attribute CO₂ emissions from petroleum and natural gas combustion from the $\delta^{13}C$ measurements. Curves showing annual averages of C_{ff} , C_{pet} , and C_{ng} , from the seasonal values from Fig. 6b are shown as thinner lines. The error bars on the results from the flask sample data are 1σ standard errors of the means. The annual emissions from the bottom-up CARB inventory are plotted using a scaling factor of 10 Tg a^{-1} for easy comparison in the plot, showing that the relative proportions are very similar through 2013.

using different $\Delta^{14}C$ for cool vs. summer months relative to the constant average value is 0.1 ppm C_{ff} .

The timing of the drop in the fossil-fuel CO₂ excess around 2008 is consistent with the economic recession in late 2007–2009 (NBER, 2010) with slow recovery beginning in 2010. Similar results for global CO₂ emissions due to fossil fuel combustion have been documented by Peters et al. (2012) and Asefi-Najafabady et al. (2014). The fraction of decrease in C_{ff} (9.5%) is similar to, although less than, the decrease in global GDP during this time (global GDP decreased by 13%; World Bank, 2015).

3.4.2 Comparison with inventories and bottom-up gridded C_{ff} data

A major goal of this study is to compare trends in top-down measurements such as those described here with bottom-up estimates in order to understand how to bring them together in space and time for direct validation. Annual averages of the seasonal amounts derived for C_{ff} , C_{pet} , and C_{ng} compare well in relative proportions to the averages from California's state inventory provided by the California Air Resources Board (CARB, 2015). Annual values for CO₂ emissions from all fossil fuels, on-road transportation, and natural gas consumption for the entire state of California, through 2013, are superimposed on the seasonal averages for C_{ff} , C_{pet} , and C_{ng} in Fig. 11. The decrease in total fossil fuels combustion between 2007 and 2011 in the State's inventory is 11%, very similar to the 9.5% decrease indicated by the EEMD time series analysis of our C_{ff} results above. There is a difference in timing between the data presented here (2010) and those from the CARB inventory (2011–2012) that may

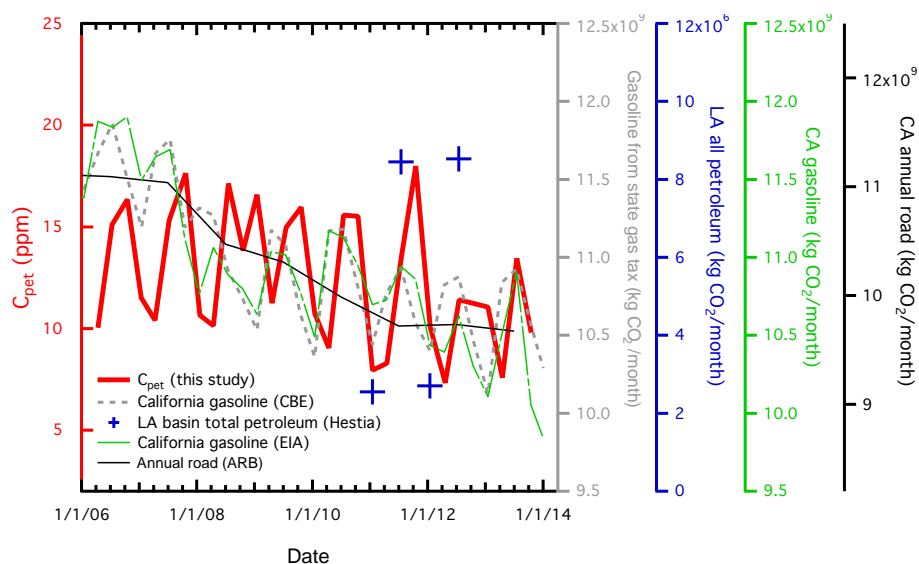


Figure 12. Comparison of the Pasadena C_{pet} atmospheric concentration with all available area-integrated bottom-up fossil fuel CO₂ emissions per month, including gasoline sales based on taxes paid to the California Board of Equalization (CBE, 2014), gasoline provided in California by prime suppliers, the California Air Resources Board's annual road emissions (CARB, 2015), and the Hestia-LA gridded total petroleum. The Hestia-LA data product is specific to the Los Angeles megacity domain; all inventories are statewide estimates. Since the Hestia-LA product is gridded, we show the emissions emanating from different regions for January (northeast quadrant, Fig. 13a) and July (southwest quadrant), based on prevailing winds during those periods (Figs. 7 and 13a). The axis for each inventory has been adjusted to allow easy comparison. The seasonality of the C_{pet} data lags the bottom-up inventories by a few months. This analysis is consistent with the observed decrease in gasoline combustion during 2008–2011.

be due to uncertainties in the data or to the different domains covered by the two data sets. The relative proportions of the on-road portion of the CARB budget is 57 % of fossil fuel CO₂ emissions and the petroleum portion of our top-down estimate averages 54 % of C_{ff} . This inventory is for the entire state, not the LA basin, and it includes annual values only. This discussion has focused on inter-annual variations in C_{ff} , although, as we have shown in Figs. 7 and 8, there are at least seasonal variations in wind direction. Looking at back trajectories from the entire time period of this study, we see no significant shifts in the winds, from year to year although systematic modeling has not yet been done and is beyond the scope of this paper. Next, we look at finer spatial and temporal scales.

Seasonal variations in C_{pet} concentration at the Pasadena location can be compared to the variation in emissions compiled by various sources. Figure 12 presents a comparison of the C_{pet} concentration to the petroleum and on-road CO₂ emissions components estimated by the Energy Information Administration (EIA) (EIA, 2015), the State of California (CARB, 2015), and the Hestia-LA project (K. R. Gurney, personal communication, 2015). Comparison of the seasonal averages for petroleum consumption data, based on deliveries (EIA), and gasoline taxes collected (CBE, 2014) with C_{pet} indicates similar decreases of 10–20 %, but with a lag of a few months (Fig. 12). The lag could be due to the different domains of the data sets: EIA and State of California data re-

fect the entire state domain while the Hestia C_{ff} data product reflects the LA Basin specifically, and the atmospheric data presented here represents air sampled in Pasadena.

To truly understand the observations in Pasadena, we must combine information from spatial and temporal meteorological and C_{ff} databases, such as the information obtained using a model like the Weather Research and Forecasting (WRF) model. Since this is beyond the scope of this work, we have used the information from HYSPLIT back trajectories (Fig. 7; January and July) to provide rough limits for winds arriving in Pasadena at our sampling time of 14:00 PST. These back trajectories suggest that prevailing winds during the summer come from the southwest, across the basin, and winds during the winter come from the northeast, across the mountains from the desert. We have looked at 1.3 km × 1.3 km gridded C_{ff} from the Hestia-LA data product to qualitatively determine what relative emissions from petroleum combustion are expected during January and July for the 2 years of the Hestia data (2011 and 2012). These are plotted in Fig. 12 and agree in seasonality with the observations presented here: more C_{pet} is observed during the summer than during the winter. A map of the regions selected for January (NE) and July (SW) is presented in Fig. 13a, along with the HYSPLIT back trajectories for January and July 2011, and the monthly average CO₂ emissions due to total petroleum combustion (the Hestia-LA product) from the

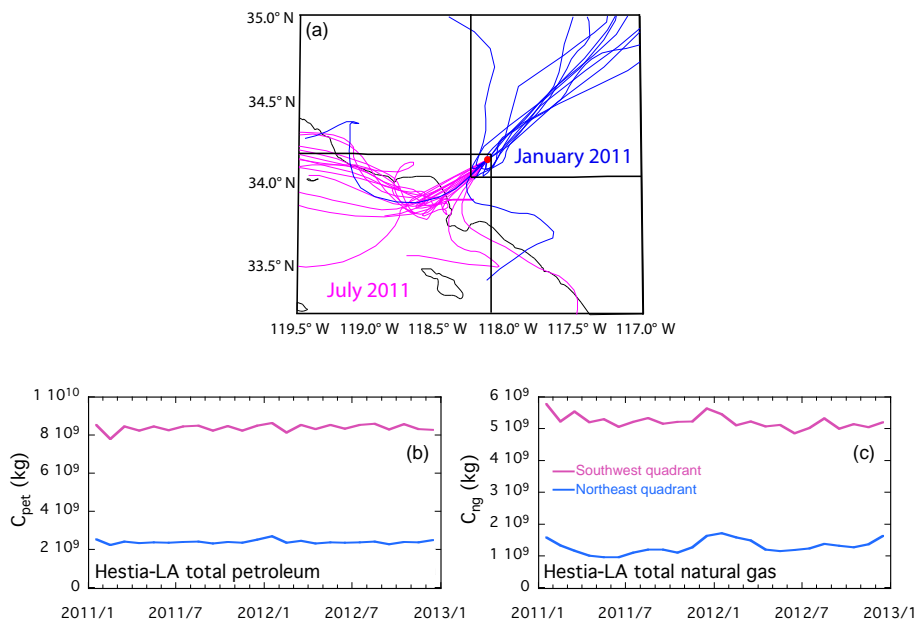


Figure 13. Relevant emissions selection from the Hestia-LA data product. **(a)** Quadrants selected for investigation of CO₂ emissions from the Hestia-LA data product, together with the 24-h back trajectories calculated by HYSPLIT for January (northeast quadrant) and July (southwest quadrant) $\Delta^{14}\text{C}$ sampling days. The back trajectories end in Pasadena (red dot) at 14:00 PST. Monthly averaged time series for Hestia-LA data product C_{ff} are shown from total petroleum combustion **(b)** and total natural gas combustion **(c)** for 2011 and 2012. For both the northeast quadrant of the Los Angeles region, the source of winter emissions, and the southwest quadrant, the source of summer emissions, the seasonal pattern is either flat (petroleum) or characterized by peaks during the winter (natural gas). But the summer emissions are always higher than those during winter, consistent with the observed top-down patterns for C_{pet} and C_{ng} in Pasadena.

two integrated areas based on the wind directions are shown in Fig. 13b for years 2011 and 2012.

We show comparison of the C_{ng} results from Pasadena with area-integrated bottom-up inventories and the Hestia-LA data product in Fig. 14. The California Energy Commission (CEC, 2015) compiles data for natural gas consumed by power plants throughout the state, including Los Angeles and Orange counties. These seasonal data are consistent with the detailed Hestia-LA data for the electricity production for the entire Los Angeles basin (dashed dark blue line in Fig. 14a). And the seasonality of all of the inventories involving just the electrical power sector agrees well with the seasonality of the time series for C_{ng} (Fig. 14a), with peaks during the summer and troughs during the winter. The source attribution analysis using $\Delta^{14}\text{C}$ and $\delta^{13}\text{C}$ also captures the increase in C_{ng} consumption of the power plants in recent years, although the data from this study suggest that the increase started earlier than the inventories. However, the observations of CO₂ concentration and $\delta^{13}\text{C}$ integrate over all natural gas combustion and cannot pick out just this one sector.

Overall statewide and Los Angeles basin inventories show maximum natural gas usage during the winter (dashed green line in Fig. 14b). Other sources of combusted natural gas include residential, commercial, industrial, and transportation use, which could affect the trends, but we do not have seasonal data for these in the Los Angeles megacity for the

full period of this study. However, the seasonal signal for total emissions from natural gas combustion from the Hestia-LA project for 2011–2012 is consistent with the data presented here, when the seasonal prevailing wind directions are considered. The seasonal pattern of emissions from natural gas combustion at any one location is characterized by a small peak during the cooler months and a trough during the warmer months (Fig. 13c). However, C_{ff} in the region sampled by winds arriving in Pasadena during the winter (the northeast) are always lower than those in the basin, over which the summer winds travel to the sampling site. Therefore, transport of air masses following the seasonal wind patterns can explain the observations in Pasadena. The earlier onset of the increase in C_{ff} from natural gas combustion indicated by the data (2010) relative to that indicated by the government inventories might be due to the mismatch in geographical regions, variations in inter-annual atmospheric transport, or deficiencies in the inventories.

Since the seasonal cycle observed in C_{pet} and C_{ng} in Pasadena is probably due to atmospheric transport, modeling of this effect is critical to being able to combine top-down observations and bottom-up economic and usage data for a direct consistency comparison. These effects must be removed in order to understand long-term trends due to variations in anthropogenic emissions. The time series analysis using empirical mode decomposition presented in Sect. 3.4.1 removes

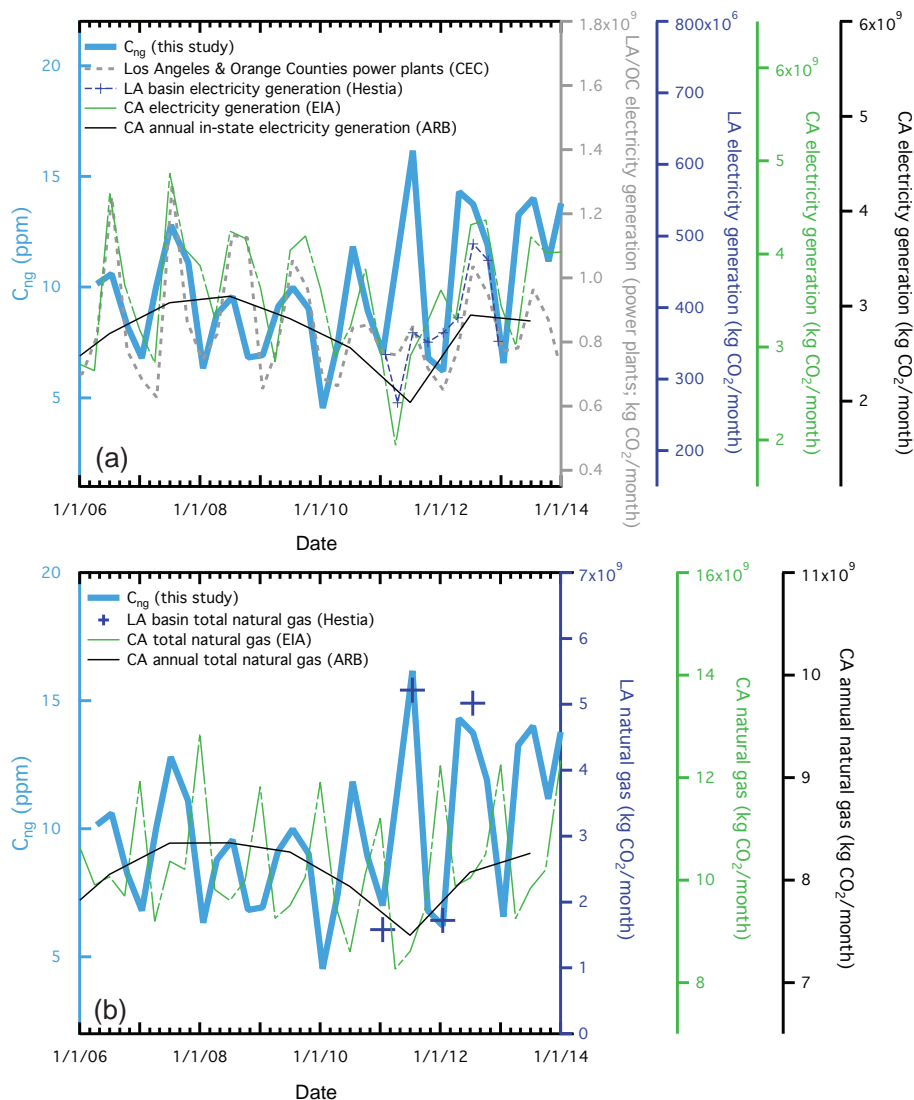


Figure 14. Comparison of Pasadena C_{ng} atmospheric concentration with area-integrated inventories of natural gas combustion, as well as the gridded Hestia-LA data product for southwest and northeast regional sectors for July and January months, respectively, in emissions/month (mo). Panel (a) compares the data from this paper with usage of natural gas by the electrical power sector; (b) shows the comparison with total natural gas consumption. Statewide inventories are given by EIA (2014) and CARB (2015) curves. Regional inventories include Hestia results and natural gas from power plants (CEC, 2014) in Los Angeles and Orange counties with monthly data (except Calabasas and Valencia). The vertical axes have been adjusted to allow easy comparison. This analysis is consistent with the increase in natural gas usage during the last few years.

the seasonal signals to concentrate on the longer-term signals, which show reasonable agreement with the longer-term trends in the statewide inventory.

4 Conclusion

Detection of anthropogenic excess of CO₂ at two sites in the Los Angeles basin, one on the coast and one inland against a barrier mountain range, reveals significant spatial and seasonal variability due to the biosphere, natural gas combustion, and petroleum combustion. Seasonal patterns in wind

direction determine the source region of the excess detected at the two sites. Winds from the west to southwest during the warmer months bring marine air with little excess to Palos Verdes, and these same winds continue across the LA basin picking up emissions from fossil fuel combustion to be observed in Pasadena. During the cooler months, wind directions are more varied and include periods when air with low emissions comes to Pasadena from the northeast to northwest and then travels across the basin to Palos Verdes, incorporating anthropogenic emissions along the way.

The nature of the excess changes with season, as reflected by the $\delta^{13}\text{C}$ values of CO₂ observed in Pasadena. During warmer months, lower values for $\delta^{13}\text{C}$ of the local excess indicate a higher proportion of natural gas burned, consistent with government inventories that indicate more natural gas burned during summer to produce electricity to power air conditioning. Even more importantly, however, the seasonal trends in the fossil fuel combustion observed in Pasadena are consistent with the shift from southwesterly winds during warmer months to northeasterly winds during cooler months. Therefore the source region of emissions changes from the Los Angeles basin during summer to the mountains and desert during winter, for our Pasadena sampling site. Trend analysis by ensemble empirical mode decomposition supports the relationship between emissions and temperature.

The long-term trend in CO₂ excess from fossil fuel combustion is consistent with C_{ff} changes associated with the economic recession and slow recovery of 2008 through the present, and indicates a significant decrease of 9.5 % since the maximum in late 2007, consistent with the bottom-up inventory of the California Air Resources Board. Indeed, top-down and bottom-up methods of determining the anthropogenic sources of CO₂ emissions must be compared to each other to better understand inconsistencies, potential biases, and uncertainty. Previously, however, comparisons have been limited by the scope of emissions, large and overlapping uncertainty, and differences in the target domain. Here we have shown that combining data from radiocarbon and $\delta^{13}\text{C}$ values moves us towards a direct comparison in a megacity with

very large emissions. Measurement trends at a receptor site are consistent with annual variations in California statewide bottom-up inventories for C_{ff} attributed to petroleum and natural combustion, individually as well as for total CO₂ emissions. Even greater consistency between top-down measurements and granular emission estimates specific for the LA megacity domain are achieved when considering wind direction and sub-city source regions. This strengthens the need to have measurement, modeling, and inventories that are specifically aimed at the same domain with fine space and/or time resolution.

The next steps are to include modeling with inversion of the measurements to understand the combination of atmospheric transport and emissions and to extend the analysis to a denser network of surface monitoring stations such as the Los Angeles Megacities Carbon Monitoring Project (Kort et al., 2013) and the California Laboratory for Atmospheric Remote Sensing (CLARS) observations from Mount Wilson (Wong et al., 2015). Although the uncertainties are large enough that the method described here will not be usable in non-urban regions, similar to the conclusion of the modeling study by Vardag et al. (2015), anthropogenic C_{ff} dominate significantly over natural processes in megacities. Therefore, this kind of monitoring in megacities will allow society to understand and monitor the sources of the CO₂ that are the major contributors to global warming.

Appendix A: Monthly Miller–Tans plots for 2011

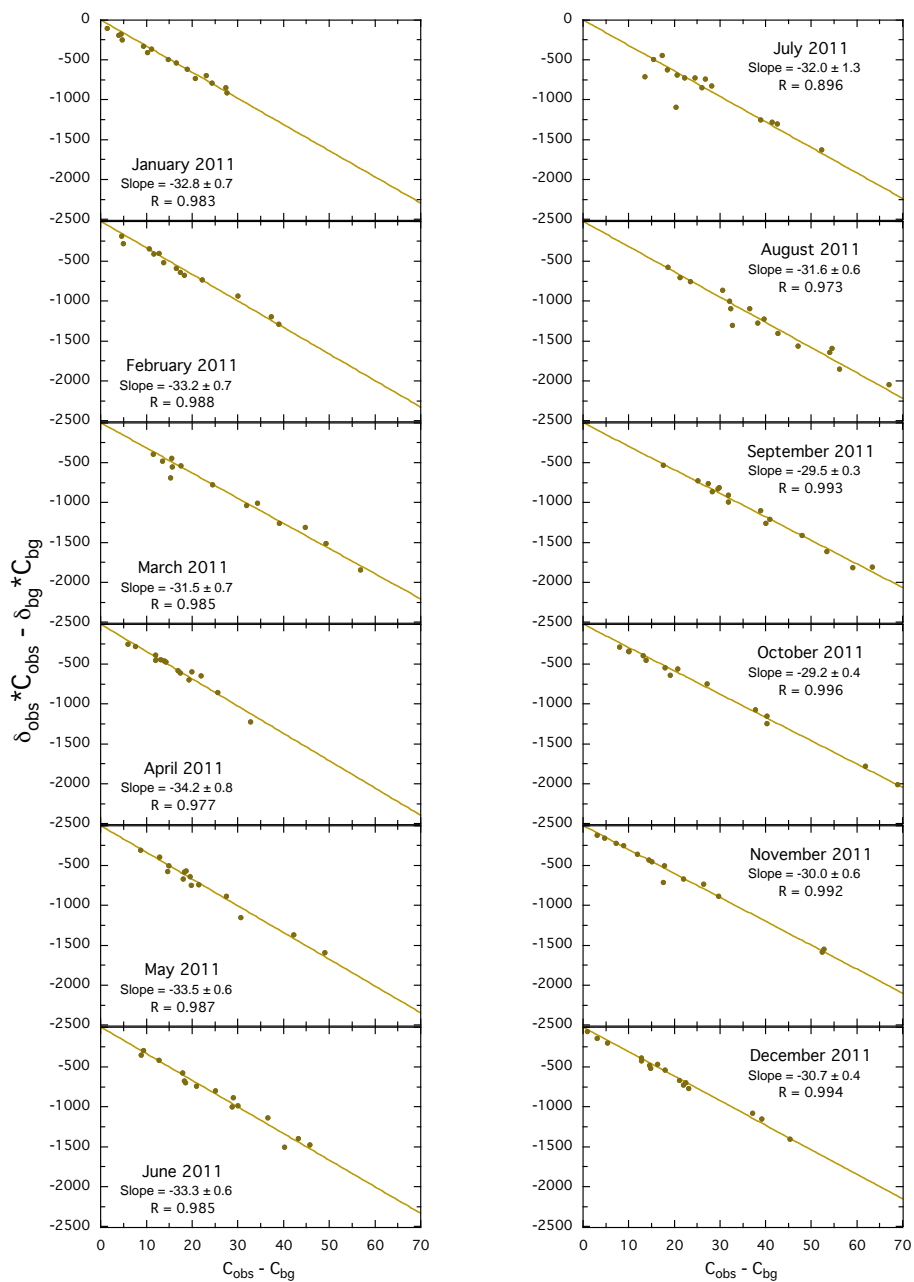


Figure A1. Miller–Tans plots for each month in 2011. Values of the slopes for 3-month seasonal averages are plotted in Fig. 6a.

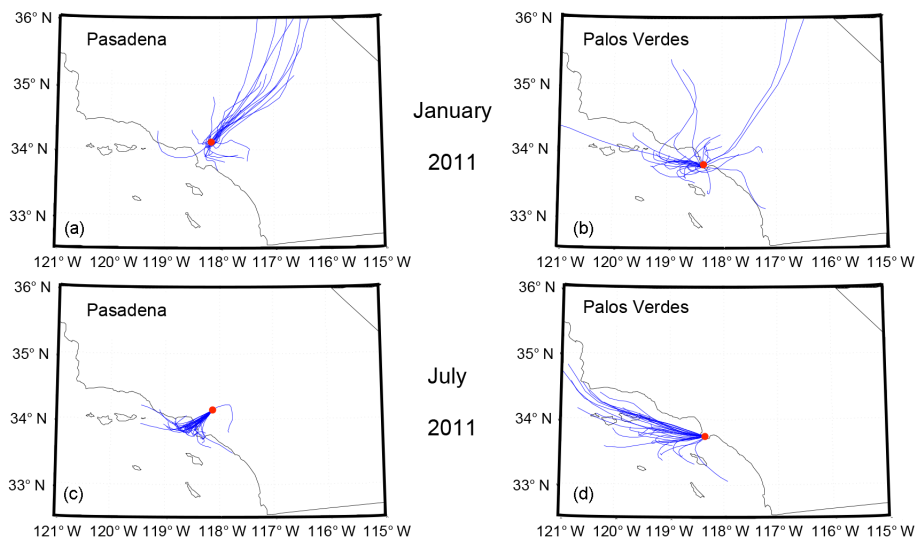
Appendix B: Back trajectories for both Pasadena and Palos Verdes sites

Figure B1. Twelve-hour back trajectories for all days in January and July 2011, for the Pasadena and Palos Verdes sites. This shows more detail for the effect of transport on the air masses sampled during summer and winter at the Palos Verdes site than Fig. 7.

Appendix C: Full ensemble empirical mode decomposition results

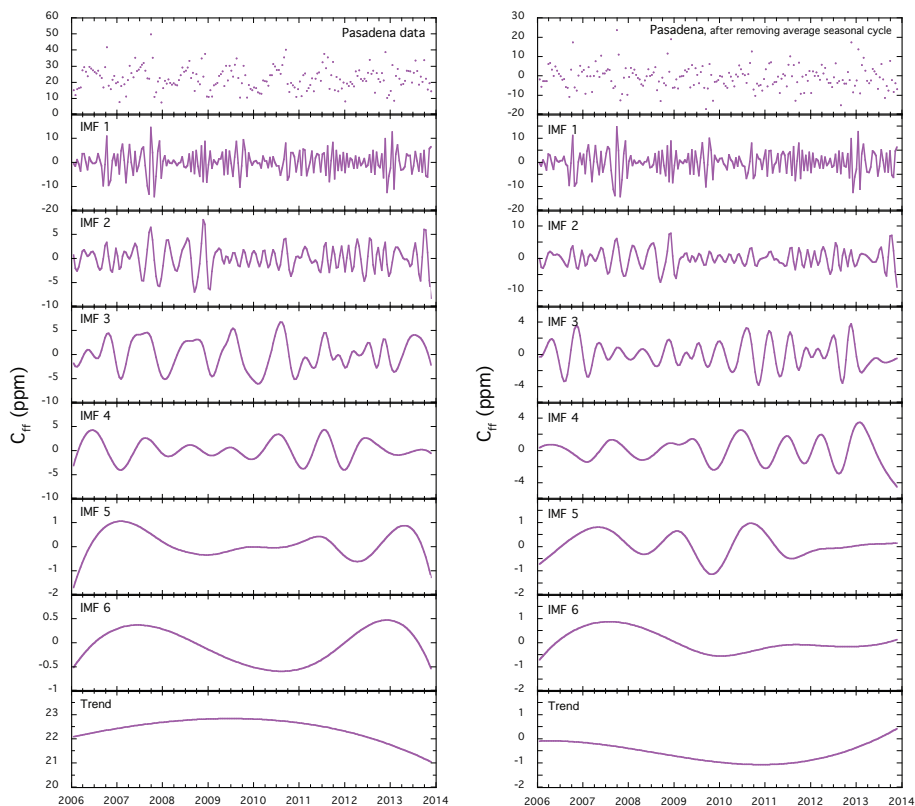


Figure C1. Time series of all of the results from the ensemble empirical mode decomposition (EEMD) analysis of the Pasadena C_{ff} . The left set of panels shows the results for the raw data, whereas the right column shows those for the data after subtraction of the average seasonal cycle. The long-term trend reflecting the economic downturn of the Great Recession is reflected clearly in IMF 6 and the trend of the data after the pronounced seasonality is removed (right-hand column), although there is some evidence of it in IMF 6 of the raw C_{ff} data.

The Supplement related to this article is available online at doi:10.5194/acp-16-3843-2016-supplement.

Acknowledgements. This work would not have been possible without support from the W. M. Keck Carbon Cycle Facility at UCI. We specifically thank J. Southon for his help with sample analysis. We acknowledge funding from the Keck Institute for Space Studies, NASA Grant NNX13AC04G, and NASA Grant NNX13AK34G. We also acknowledge funding from the California Air Resources Board Contract #13-329. The statements and conclusions in this report are those of the Contract and not necessarily those of the California Air Resources Board. The mention of commercial products, their source, or their use in connection with materials reported herein is not to be construed as actual or implied endorsement of such products. The authors gratefully acknowledge the NOAA Air Resources Laboratory (ARL) for providing the HYSPLIT transport and dispersion model used in this publication. We thank N. C. Shu for hosting the site on the Palos Verdes peninsula.

Edited by: J. Kaiser

References

- Andres, R. J., Boden, T. A., Bréon, F.-M., Ciais, P., Davis, S., Erickson, D., Gregg, J. S., Jacobson, A., Marland, G., Miller, J., Oda, T., Olivier, J. G. J., Raupach, M. R., Rayner, P., and Treanton, K.: A synthesis of carbon dioxide emissions from fossil-fuel combustion, *Biogeosciences*, 9, 1845–1871, doi:10.5194/bg-9-1845-2012, 2012.
- Affek, H. and Eiler, J.: Abundance of mass 47 CO₂ in urban air, car exhaust, and human breath, *Geochim. Cosmochim. Ac.*, 70, 1–12, 2006.
- Affek, H., Xu, X., and Eiler, J.: Seasonal and diurnal variations of ¹³C¹⁸O¹⁶O in air: Initial observations from Pasadena, CA, *Geochim. Cosmochim. Ac.*, 71, 5033–5043, doi:10.1016/j.gca.2007.08.014, 2007.
- Asefi-Najafabady, S., Rayner, P. J., Gurney, K. R., McRobert, A., Song, Y., Coltin, K., Huang, J., Elvidge, C., and Baugh, K.: A multiyear, global gridded fossil fuel CO₂ emission data product: Evaluation and analysis of results, *J. Geophys. Res.-Atmos.*, 119, 10213–10231, doi:10.1002/2013JD021296, 2014.
- Bakwin, P., Tans, P., White, J., and Andres, R.: Determination of the isotopic (¹³C/¹²C) discrimination by terrestrial biology from a global network of observations, *Global Biogeochem. Cy.*, 12, 555–562, 1998.
- Bush, S., Pataki, D., and Ehleringer, J.: Sources of variation in δ¹³C of fossil fuel emissions in Salt Lake City, USA, *Appl. Geochem.*, 2, 715–723, doi:10.1016/j.apgeochem.2006.11.001, 2007.
- CARB, California Air Resources Board: available at: <http://www.arb.ca.gov/cc/inventory/data/data.htm>, last access: July 2015.
- CBE, California Board of Equalization: available at: http://www.boe.ca.gov/sptaxprog/reports/MVF_10_Year_Report.pdf, last access: November 2014.
- CEC, California Energy Commission: available at: http://energyalmanac.ca.gov/electricity/web_qfer/Power_Plant_Statistical_Information.php, last access: January 2015.
- Clark-Thorne, S. and Yapp, C.: Stable carbon isotope constraints on mixing and mass balance of CO₂ in an urban atmosphere: Dallas metropolitan area, Texas, USA, *Appl. Geochem.*, 18, 75–95, 2003.
- Conil, S. and Hall, A.: Local regimes of atmospheric variability: A case study of southern California, *J. Climate*, 19, 4308–4325, 2006.
- Coplen, T. B.: Editorial: more uncertainty than necessary, *Paleoceanography*, 11, 369–370, 1996.
- Djuricin, S., Pataki, D. E., and Xu, X.: A comparison of tracer methods for quantifying CO₂ sources in an urban region, *J. Geophys. Res.-Atmos.*, 115, D11303, doi:10.1029/2009JD012236, 2010.
- Draxler, R. R. and Rolph: G. D.: HYSPLIT (HYbrid Single-Particle Lagrangian Integrated Trajectory) Model access via NOAA ARL READY Website (<http://www.arl.noaa.gov/HYSPLIT.php>), NOAA Air Resources Laboratory, College Park, MD, USA, 2014.
- Duren, R. M. and Miller, C. E.: Measuring the carbon emissions of megacities, *Nature Climate Change*, 2, 560–562, 2012.
- EDGAR: European Commission, Joint Research Centre (JRC)/Netherlands Environmental Assessment Agency (PBL). Emission Database for Global Atmospheric Research (EDGAR), release version 4.0. available at: <http://edgar.jrc.ec.europa.eu> (last access: September 2015), 2009.
- EIA (U.S. Energy Information Agency): Frequently asked questions: available at: <http://www.eia.gov/tools/faqs/faq.cfm?id=307&t=11>, last access: 4 September 2015.
- Farquhar, G., Ehleringer, J. R., and Hubick, K. T.: Carbon isotope discrimination and photosynthesis, *Annu. Rev. Plant. Phys.*, 40, 503–537, 1989.
- Graven, H., Xu, X., Guilderson, T. P., and Keeling R. F.: Comparison of independent Δ¹⁴CO₂ records at Point Barrow, Alaska, *Radiocarbon*, 55, 1541–1545, 2013.
- Graven, H. D. and Gruber, N.: Continental-scale enrichment of atmospheric ¹⁴CO₂ from the nuclear power industry: potential impact on the estimation of fossil fuel-derived CO₂, *Atmos. Chem. Phys.*, 11, 12339–12349, doi:10.5194/acp-11-12339-2011, 2011.
- Graven, H. D., Guilderson, T. P., and Keeling, R. F.: Observations of radiocarbon in CO₂ at La Jolla, California, USA 1992–2007: Analysis of the long-term trend, *J. Geophys. Res.*, 117, D02302, doi:10.1029/2011JD016533, 2012.
- Gurney, K., Mendoza, D., Zhou, Y., Fischer, M., Miller, C., Geethakumar, S., and du Can, S.: High Resolution Fossil Fuel Combustion CO₂ Emission Fluxes for the United States, *Environ. Sci. Technol.*, 43, 5535–5541, doi:10.1021/es900806c, 2009.
- Gurney, K. R., Razlivanov, I., Song, Y., Zhou, Y., Benes, B., and Abdul-Massin, M.: Quantification of fossil fuel CO₂ emissions on the building/street scale for a large U.S. city, *Environ. Sci. Technol.*, 46, 12194–12202, doi:10.1021/es3011282, 2012.
- Gurney, K. R., Romero-Lankao, P., Seto, K. C., Hutyra, L. R., Duren, R., Kennedy, C., Grimm, N. B., Ehleringer, J. R., Marcutuillio, P., Hughes, S., Pincetl, S., Chester, M. V., Runfola, D. M., Feddema, J. J., and Sperling, J.: Climate change: Track urban emissions on a human scale, *Nature*, 525, 179–181, doi:10.1038/525179a, 2015.
- Huang, N., Shen, Z., and Long, S.: The empirical mode decomposition and the Hilbert spectrum for nonlinear and non-stationary

- time series analysis, *Proc. R. Soc. Lon, Ser.-A*, 454, 903–995, 1998.
- IEA: World Energy Outlook 2008, edited by: Birol, F., International Energy Agency, Paris, France, 2008.
- IPCC: Climate Change 2013: The Physical Science Basis. Contribution of Working Group I to the Fifth Assessment Report of the Intergovernmental Panel on Climate Change, edited by: Stocker, T. F., Qin, D., Plattner, G.-K., Tignor, M., Allen, S. K., Boschung, J., Nauels, A., Xia, Y., Bex, V., and Midgley, P. M., Cambridge University Press, Cambridge, UK and New York, NY, USA, 1535 pp., 2013.
- Jacobson, M. Z.: On the causal link between carbon dioxide and air pollution mortality, *Geophys. Res. Lett.*, 35, L03809, doi:10.1029/2007GL031101, 2008.
- Jiang, X., Li, Q., Liang, M.-C., Shia, R.-L., Chahine, M. T., Olsen, E. T., Chen, L. L., and Yung, Y. L.: Simulation of upper tropospheric CO₂ from chemistry and transport models, *Global Biogeochem. Cy.*, 22, GB4025, doi:10.1029/2007GB003049, 2008.
- Jiang, X., Chahine, M. T., Li, Q., Liang, M., Olsen, E. T., Chen, L. L., Wang, J., and Yung, Y. L.: CO₂ semiannual oscillation in the middle troposphere and at the surface, *Global Biogeochem. Cy.*, 26, GB3006, doi:10.1029/2011GB004118, 2012.
- Keeling, C.: The concentration and isotopic abundances of carbon dioxide in rural and marine air, *Geochim. Cosmochim. Ac.*, 24, 277–298, 1961.
- Keeling, C. D.: The concentration and isotopic abundances of atmospheric carbon dioxide in rural areas, *Geochim. Cosmochim. Ac.*, 13, 322–334, doi:10.1016/0016-7037(58)90033-4, 1958.
- Keeling, C. D., Piper, S. C., Bacastow, R. B., Wahlen, M., Whorf, T. P., Heimann, M., and Meijer, H. A.: Atmospheric CO₂ and ¹³C exchange with the terrestrial biosphere and oceans from 1978 to 2000: observations and carbon cycle implications, in: *A History of Atmospheric CO₂ and its effects on Plants, Animals, and Ecosystems*, edited by: Ehleringer, J. R., Cerling, T. E., and Dearing, M. D., Springer Verlag, New York, USA, 83–113, 2005.
- Kobayashi-Kirschvink, K. J., Li, K.-F., Shia, R.-L., and Yung, Y. L.: Fundamental modes of atmospheric CFC-11 from empirical mode decomposition, *Adv. Adapt. Data Anal.*, 4, 1250024, doi:10.1142/S1793536912500240, 2012.
- Kort, E. A., Angevine, W., Duren, R., and Miller, C. E.: Surface observations for monitoring urban fossil fuel CO₂ emissions: minimum site location requirements for the Los Angeles megacity, *J. Geophys. Res.*, 118, 1–8, doi:10.1002/jgrd.50135, 2013.
- Levin, I. and Roedenbeck, C.: Can the envisaged reductions of fossil fuel CO₂ emissions be detected by atmospheric observations?, *Naturwissenschaften*, 95, 203–208, doi:10.1007/s00114-007-0313-4, 2008.
- Levin, I., Kromer, B., Schmidt, M., and Sartorius, H.: A novel approach for independent budgeting of fossil fuel CO₂ over Europe by ¹⁴CO₂ observations, *Geophys. Res. Lett.*, 30, 2194, doi:10.1029/2003GL018477, 2003.
- Lopez, M., Schmidt, M., Delmotte, M., Colomb, A., Gros, V., Janssen, C., Lehman, S. J., Mondelain, D., Perrussel, O., Ramonet, M., Xueref-Remy, I. and Bousquet, P.: CO, NO_x and ¹³CO₂ as tracers for fossil fuel CO₂: results from a pilot study in Paris during winter 2010, *Atmos. Chem. Phys.*, 13, 7343–7358, doi:10.5194/acp-13-7343-2013, 2013.
- Lu, R. and Turco, R.: Air pollutant transport in a coastal environment. Part I: Two-dimensional simulations of sea-breeze and mountain effects, *J. Atmos. Sci.*, 51, 2285–2308, 1994.
- Lu, R. and Turco, R.: Air pollutant transport in a coastal environment – II. Three-dimensional simulations over Los Angeles basin, *Atmos. Environ.*, 29, 1499–1518, 1995.
- Moore, J. and Jacobson, A. D.: Seasonally varying contributions to urban CO₂ in the Chicago, Illinois, USA region: Insights from a high-resolution CO₂ concentration and δ¹³C record, *Elem. Sci. Anth.*, 3, 000052, doi:10.12952/journal.elementa.000052.s004, 2015.
- Miller, J. and Tans, P.: Calculating isotopic fractionation from atmospheric measurements at various scales, *Tellus B*, 55, 207–214, 2003.
- Miller, J., Lehman, S., Wolak, C., Turnbull, J., Dunn, G., Graven, H., Keeling, R., H. Meijer, A., Aerts-Bijma, A. T., and Palstra, S. W.: Initial results of an intercomparison of AMS-based atmospheric ¹⁴CO₂ measurements, *Radiocarbon*, 55, 1475–1483, 2013.
- Miller, J. B., Lehman, S. J., Montzka, S. A., Sweeney, C., Miller, B. R., Karion, A., Wolak, C., Dlugokencky, E. J., Southon, J., Turnbull, J. C., and Tans, P. P.: Linking emissions of fossil fuel CO₂ and other anthropogenic trace gases using atmospheric ¹⁴CO₂, *J. Geophys. Res.*, 117, D08302, doi:10.1029/2011JD017048, 2012.
- NBER, National Bureau of Economic Research: available at: <http://www.nber.org/cycles/sept2010.html>, last access: September 2010.
- Newman, S., Xu, X., Affek, H. P., Stolper, E., and Epstein, S.: Changes in mixing ratio and isotopic composition of CO₂ in urban air from the Los Angeles basin, California, between 1972 and 2003, *J. Geophys. Res.-Atmos.*, 113, D23304, doi:10.1029/2008JD009999, 2008.
- Newman, S., Jeong, S., Fischer, M. L., Xu, X., Haman, C. L., Lefer, B., Alvarez, S., Rappenglueck, B., Kort, E. A., Andrews, A. E., Peischl, J., Gurney, K. R., Miller, C. E., and Yung, Y. L.: Diurnal tracking of anthropogenic CO₂ emissions in the Los Angeles basin megacity during spring 2010, *Atmos. Chem. Phys.*, 13, 4359–4372, doi:10.5194/acp-13-4359-2013, 2013.
- NRC, National Research Council: *Advancing the Science of Climate Change*, National Research Council, The National Academies Press, Washington, DC, USA, 2010.
- Pataki, D., Bowling, D., and Ehleringer, J.: Seasonal cycle of carbon dioxide and its isotopic composition in an urban atmosphere: Anthropogenic and biogenic effects, *J. Geophys. Res.*, 108, 4735, doi:10.1029/2003JD003865, 2003.
- Patarasuk, R., Gurney, K. R., O’Keeffe, D., Song, Y., Huang, J., Rao, P., Buchert, M., Lin, J., Mendoza, D., and Ehleringer, J.: High-resolution fossil fuel CO₂ emissions quantification and application to urban climate policy, *Urban Ecosys.*, accepted, 2016.
- Peters, G., Marland, G., Le Quééré, C., and Boden, T.: Rapid growth in CO₂ emissions after the 2008–2009 global financial crisis, *Nature Climate Change*, 2, 2–4, 2012.
- Prinn, R. G., Weiss, R. F., Fraser, P. J., Simmonds, P. G., Cunnold, D. M., Alyea, F. N., O’Doherty, S., Salameh, P., Miller, B. R., Huang, J., Wang, R., Hartley, D. E., Harth, C., Steele, L. P., Sturrock, G., Midgley, P. M., and McCulloch, A.: A history of chemically and radiatively important gases in air deduced from ALE/GAGE/AGAGE, *J. Geophys. Res.-Atmos.*, 105, 17751–17792, doi:10.1029/2000JD900141, 2000.

- Raphael, M.: The Santa Ana winds of California, *Earth Interact.*, 7, 1–13, 2003.
- Rolph, G. D.: Real-time Environmental Applications and Display sYstem (READY) Website: available at: <http://www.ready.noaa.gov> (last access: July 2015), NOAA Air Resources Laboratory, College Park, MD, USA, 2014.
- Thoning, K., Tans, P., and Komhyr, W.: Atmospheric carbon dioxide at Mauna Loa Observatory, 2, Analysis of the NOAA/GMCC data, 1974–1985, *J. Geophys. Res.*, 94, 8549–8565, 1989.
- Turnbull, J., Miller, J., Lehman, S., Tans, P., Sparks, R., and Southon, J.: Comparison of ¹⁴CO₂, CO, and SF₆ as tracers for recently added fossil fuel CO₂ in the atmosphere and implications for biological CO₂ exchange, *Geophys. Res. Lett.*, 33, L01817, doi:10.1029/2005GL024213, 2006.
- Turnbull, J., Rayner, P., Miller, J., Naegler, T., Ciais, P., and Cozic, A.: On the use of (CO₂)-C-14 as a tracer for fossil fuel CO₂: Quantifying uncertainties using an atmospheric transport model, *J. Geophys. Res.-Atmos.*, 114, D22302, doi:10.1029/2009JD012308, 2009.
- Turnbull, J. C., Karion, A., Fischer, M. L., Faloona, I., Guilderson, T., Lehman, S. J., Miller, B. R., Miller, J. B., Montzka, S., Sherwood, T., Saripalli, S., Sweeney, C., and Tans, P. P.: Assessment of fossil fuel carbon dioxide and other anthropogenic trace gas emissions from airborne measurements over Sacramento, California in spring 2009, *Atmos. Chem. Phys.*, 11, 705–721, doi:10.5194/acp-11-705-2011, 2011.
- Turnbull, J. C., Sweeney, C., Karion, A., Newberger, T., Lehman, S. J., Tans, P. P., Davis, K. J., Lauvaux, T., Miles, N. L., Richardson, S. J., Cambaliza, M. O., Shepson, P. B., Gurney, K., Patarasuk, R., and Razlivanov, I.: Toward quantification and source sector identification of fossil fuel CO₂ emissions from an urban area: Results from the INFLUX experiment, *J. Geophys. Res.-Atmos.*, 120, 292–312, doi:10.1002/2014JD022555, 2015.
- Vardag, S. N., Gerbig, C., Janssens-Maenhout, G., and Levin, I.: Estimation of continuous anthropogenic CO₂: model-based evaluation of CO₂, CO, δ¹³C(CO₂) and Δ¹⁴C(CO₂) tracer methods, *Atmos. Chem. Phys.*, 15, 12705–12729, doi:10.5194/acp-15-12705-2015, 2015.
- Widory, D. and Javoy, M.: The carbon isotope composition of atmospheric CO₂ in Paris, *Earth Planet Sc. Lett.*, 215, 289–298, 2003.
- Wong, K. W., Fu, D., Pongetti, T. J., Newman, S., Kort, E. A., Duren, R., Hsu, Y.-K., Miller, C. E., Yung, Y. L., and Sander, S. P.: Mapping CH₄:CO₂ ratios in Los Angeles with CLARS-FTS from Mount Wilson, California, *Atmos. Chem. Phys.*, 15, 241–252, doi:10.5194/acp-15-241-2015, 2015.
- World Bank: GDP, available at: <http://data.worldbank.org/indicator/NY.GDP.MKTP.CD/countries/1W-US?display=graph>, last access: May 2015.
- Wu, Z. and Huang, N. E.: Ensemble empirical mode decomposition: A noise-assisted data analysis method, *Adv. Adapt. Data Anal.*, 1, 1–41, 2009.
- Xu, X., Trumbore, S. E., Zheng, S., Southon, J. R., McDuffee, K. E., Luttgen, M., and Liu, J. C.: Modifying a sealed tube zinc reduction method for preparation of AMS graphite targets: Reducing background and attaining high precision, *Nucl. Instrum. Meth. B*, 259, 320–329, 2007.
- Xu, X., Khosh, M. S., Druffel-Rodriguez, K. C., Trumbore S. E., and Southon J. R.: Is the consensus value of ANU sucrose (IAEA C-6) too high? *Radiocarbon*, 52, 866–874, 2010.